iScience

CellPress

Article

An Ancient BCR-like Signaling Promotes ICP Production and Hemocyte Phagocytosis in Oyster

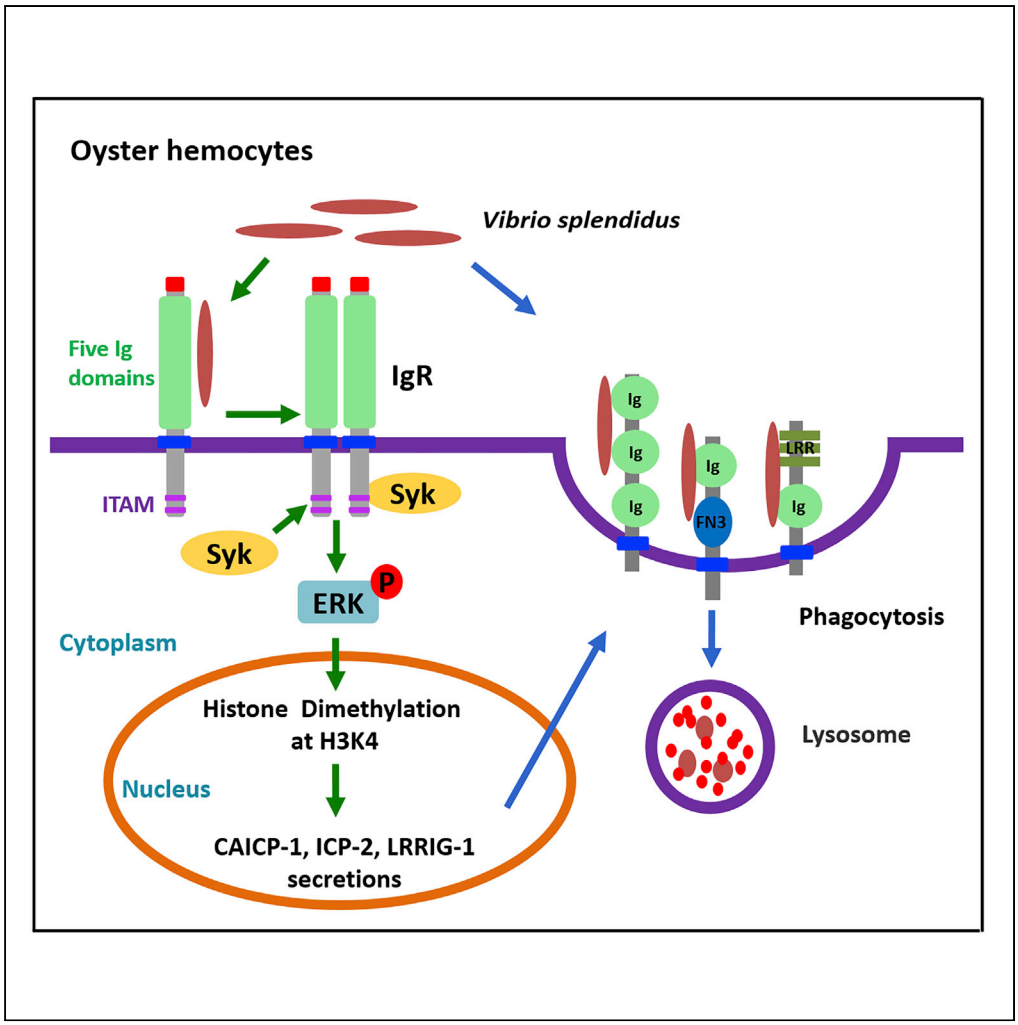

Jiejie Sun, Lingling Wang, Chuanyan Yang, Linsheng Song

wanglingling@dlou.edu.cn (L.W.)
lshsong@dlou.edu.cn (L.S.)

HIGHLIGHTS

An ancient BCR-like molecule (defined as *Cg*IgR) was identified from *C. gigas*

We propose IgR-mediated signaling induces *Cg*ERK activity in oyster

IgR-mediated signaling induced *Cg*H3K4me2 to promote the production of *Cg*ICPs

*Cg*ICPs facilitated the hemocytes to phagocytize and eliminate *V. splendidus*

Sun et al., iScience *23*, 100834
February 21, 2020
https://doi.org/10.1016/j.isci.2020.100834

iScience

CellPress

Article

An Ancient BCR-like Signaling Promotes ICP Production and Hemocyte Phagocytosis in Oyster

Jiejie Sun,[1,3] Lingling Wang,[1,2,3,4,*] Chuanyan Yang,[1,3] and Linsheng Song[1,2,3,5,*]

SUMMARY

BCR/TCR-based adaptive immune systems arise in the jawed vertebrates, and B cell receptors (BCRs) play an important role in the clonal selection of B cells and their differentiation into antibody-secreting plasma cells. The existence of BCR-like molecule and the activation mechanism of the downstream response are still not clear in invertebrates. In this study, an ancient BCR-like molecule (designated as *Cg*IgR) with an immunoreceptor tyrosine-based activation motif (ITAM) in its cytoplasmic tail was identified from the Pacific oyster *Crassostrea gigas* to investigate its involvement in immune response. *Cg*IgR could bind different bacteria through five extracellular Ig domains and formed dimers. The activated *Cg*IgR recruited *Cg*Syk to promote *Cg*ERK phosphorylation. The *Cg*IgR-mediated signaling promoted the production of immunoglobulin domain-containing proteins (*Cg*ICP-2 and *Cg*LRRIG-1) through inducing *Cg*H3K4me2. The produced *Cg*ICPs eventually facilitated hemocytes to phagocytize and eliminate *V. splendidus*. This study proposed that there was an ancient BCR-like molecule and BCR-like signaling in molluscs.

INTRODUCTION

Adaptive immunity involves a tightly regulated interplay between antigen-presenting cells and T/B cells, which facilitates pathogen-specific immunologic effector pathways, generation of immunologic memory, and regulation of immune homeostasis (Bonilla and Oettgen, 2010). B cell receptors (BCRs) are considered as the key molecules in the adaptive immunity, which can govern the initiation of transcriptional programs associated with B cell activation (Kwak et al., 2019) and then mediate the production of antibodies through plasma cells (Konigsberger et al., 2012; Mattila et al., 2013; Yang and Reth, 2010). BCRs comprise the membrane bound immunoglobulin (mIg) and the signal-transducing Igα/Igβ heterodimer, which function as the ligand-binding and signaling subunits, respectively (Monroe, 2006; Reth, 1989). The mIg recognizes various antigens via Ig domains and activates the membrane Igα and Igβ. The activated Igα and Igβ then form heterodimer to transduce signals through their immunoreceptor tyrosine-based activation motifs (ITAMs) (DeFranco, 1993; Papavasiliou et al., 1995; Teh and Neuberger, 1997). The clustering of Igα and Igβ initially stimulates the membrane-associated Src protein tyrosine kinases (PTKs) to phosphorylate the ITAM tyrosines of Igα and Igβ. The phosphorylated Igα and Igβ tyrosines then serve as membrane proximal binding sites for the tandem Src homology 2 (SH2) domains presented in spleen tyrosine kinase (Syk) (Rowley et al., 1995). This process allows Syk to bind BCRs and phosphorylate the neighboring ITAM tyrosines, thus amplifying the signaling output of the BCRs (Rolli et al., 2002). The signaling mediated by BCRs induces B cell activation, proliferation, differentiation, and eventually secretions of antibodies (Ollila and Vihinen, 2005; Werner et al., 2010). The antibodies are a class of Igs found only in vertebrates, which function in multiple biological processes such as specifically recognizing antigens, participating in neutralizing toxins, activating the complement pathway, and inducing opsonization (Panda and Ding, 2015). Although the ancestral cell lineage of Ig-producing B cells is still unknown, fish B cells are confirmed to represent the cell predecessors for amphibian, reptilian, avian, and mammalian B cells (Jirapongpairoj et al., 2017; Simon et al., 2019; Smith et al., 2019; Yu et al., 2018). However, there is still no report about BCR in fish, and the initiation mechanisms of B cells are far from well understood.

The immunological memory in invertebrates as well as the origin and evolution of immunoglobulins have been in controversy in the past decades (Chang et al., 2018; Torre et al., 2017). The memory of trained immunity is defined as a heightened response to a secondary infection (Netea et al., 2011). Although increasing evidences suggest that there exists trained immunity in invertebrates (Norouzitallab et al., 2016; Simoes and Dimopoulos, 2015), the underlying molecular and cellular mechanisms still need further

[1]Liaoning Key Laboratory of Marine Animal Immunology, Dalian Ocean University, 52 Heishijiao Street, Dalian 116023, China

[2]Laboratory of Marine Fisheries Science and Food Production Processes, Qingdao National Laboratory for Marine Science and Technology, Qingdao 266235, China

[3]Liaoning Key Laboratory of Marine Animal Immunology & Disease Control, Dalian Ocean University, Dalian 116023, China

[4]Dalian Key Laboratory of Aquatic Animal Diseases Prevention and Control, Dalian Ocean University, Dalian 116023, China

[5]Lead Contact

*Correspondence: wanglingling@dlou.edu.cn (L.W.), lshsong@dlou.edu.cn (L.S.)

https://doi.org/10.1016/j.isci.2020.100834

investigation. As the key component of adaptive immunity, antibodies are assumed to have arisen in the jawed vertebrates (Smith et al., 2019), whereas their primitive ancestors and functions in invertebrate immune system are still largely unknown. So far, numerous immunoglobulin domain-containing proteins (ICPs) with one or more Ig-like domains have been identified in invertebrates (Dong et al., 2006; Hemani and Soller, 2012; Wang et al., 2018). For instance, more than 190 ICPs were annotated in oyster *Crassostrea gigas* by screening the available genomic sequence (Zhang et al., 2015). Some of invertebrate ICPs are found to be alternatively spliced after immune stimuli, which is similar to that of antibodies in mammals (Parra et al., 2013). For example, Down syndrome cell adhesion molecule (Dscam) in *Drosophila* and mosquito could generate pathogen-splice form repertoires through alternative splicing upon immune challenge (Dong et al., 2006; Hemani and Soller, 2012). *Es*Dscam in Chinese mitten crab *Eriocheir sinensis* potentially produced 30,600 isoforms due to the alternative splice of three Ig domains, which suggested that *Es*Dscam owned specific recognition capability to different bacteria (Li et al., 2018). A cysteine-rich motif associated ICP (*Cg*CAICP-1) was also reported to be spliced in *C. gigas* (Liu et al., 2018). These evidences suggest that the diversified ICPs are created by rearrangement and enable specific recognition and protection against bacteria (Kurtz and Armitage, 2006). In most invertebrates, circulating hemocytes are the main immunocytes responsible for recognition, phagocytosis, nodule formation, encapsulation, and effector synthesis (Christophides et al., 2002; Koiwai et al., 2018; Lau et al., 2017). Many ICPs in invertebrates are found to be expressed in hemocytes and function as pattern recognition receptors (PRRs) and opsonins. For example, a junctional adhesion molecule A (*Cg*JAM-A-L) and *Cg*CAICP-1 were found to be located on the hemocyte membrane. Both of them functioned as PRRs to recognize different bacteria and facilitated phagocytosis of oyster hemocytes (Liu et al., 2016b, 2018). However, the knowledge on the origin and evolution of BCR molecule as well as their possible ligand-binding mechanism and signaling cascades to regulate other ICP production in invertebrates is still very limited.

As aquaculture mollusk, oyster is of critically evolutional significance and economic importance and represents an attractive model for studying the immune function and evolution of immune system because it is a sessile and filter-feeder always exposed to tremendous pathogen challenge (Zhang et al., 2012). Hemocytes are important in the defense mechanisms of oyster (Moreau et al., 2015; Wang et al., 2018a), and many ICPs functioning as PRRs and opsonins are highly expressed in the oyster hemocytes. Four *Cg*ICPs (*Cg*IgR, *Cg*CAICP-1, *Cg*ICP-2, and *Cg*LRRIG-1) were screened from the transcriptome data of oyster hemocytes after the successive *V. splendidus* and lipopolysaccharide (LPS) stimulations, which were suspected to be involved in the trained immunity. In the present study, an ancient BCR-like molecule (*Cg*IgR) was identified from oyster, and its recognition and regulation mechanisms to induce *Cg*ICP production and phagocytosis toward *V. splendidus* were investigated with the objectives to comprehensively understand the function of immunoglobulin domain-containing proteins in the immune system of invertebrates and provide some clues for the origin of BCR-mediated antibody secretions and the evolution of adaptive immunity.

RESULTS

The Phagocytic Rates and *Cg*ICP Transcripts Increased Significantly after the Immune Training with *V. splendidus* and LPS

The oysters were pre-stimulated with *V. splendidus* or LPS to train their immune responses. At the eighth day after the first stimulation, the oysters were stimulated again with *V. splendidus* and LPS for 6 h, respectively. Control oysters received a first injection with PBS and a second injection with *V. splendidus*. The hemocytes were collected to examine the phagocytic rates and the mRNA transcripts of *Cg*ICPs (Figure 1A). The phagocytic rates of hemocytes toward *V. splendidus* were apparently enhanced in *V. splendidus* and LPS training oysters, which were 1.58-fold and 1.52-fold ($p < 0.05$) higher than that in PBS training oysters (Figures 1B–1E). The flow cytometry assay also confirmed that the phagocytic rates of hemocytes toward *V. splendidus* increased significantly (1.73-fold and 1.79-fold of that in PBS training oysters, $p < 0.05$, respectively) in *V. splendidus* and LPS training oysters (Figure 1F). The mRNA transcripts of *Cg*ICPs (*Cg*IgR, *Cg*CAICP-1, *Cg*ICP-2, *Cg*LRRIG-1) (Figure S1) increased significantly in *V. splendidus* training oysters (3.07-fold, $p < 0.01$; 2.69-fold, 2.35-fold, and 2.16-fold, $p < 0.05$) and LPS training oysters (3.56-fold, 2.93-fold, 2.71-fold, and 1.94-fold, $p < 0.05$), compared with that in PBS training oysters, respectively (Figures 1G–1N).

No Significant Changes of Hemocyte Phagocytosis and *Cg*ICPs Transcripts Were Observed in *Cg*IgR-RNAi Oysters after the Immune Training with *V. splendidus* and LPS

The phagocytosis of oyster hemocytes and mRNA expressions of *Cg*ICPs were examined after *Cg*IgR was knocked down to study its possible function in training immunity. *Cg*IgR-RNAi oysters were first stimulated

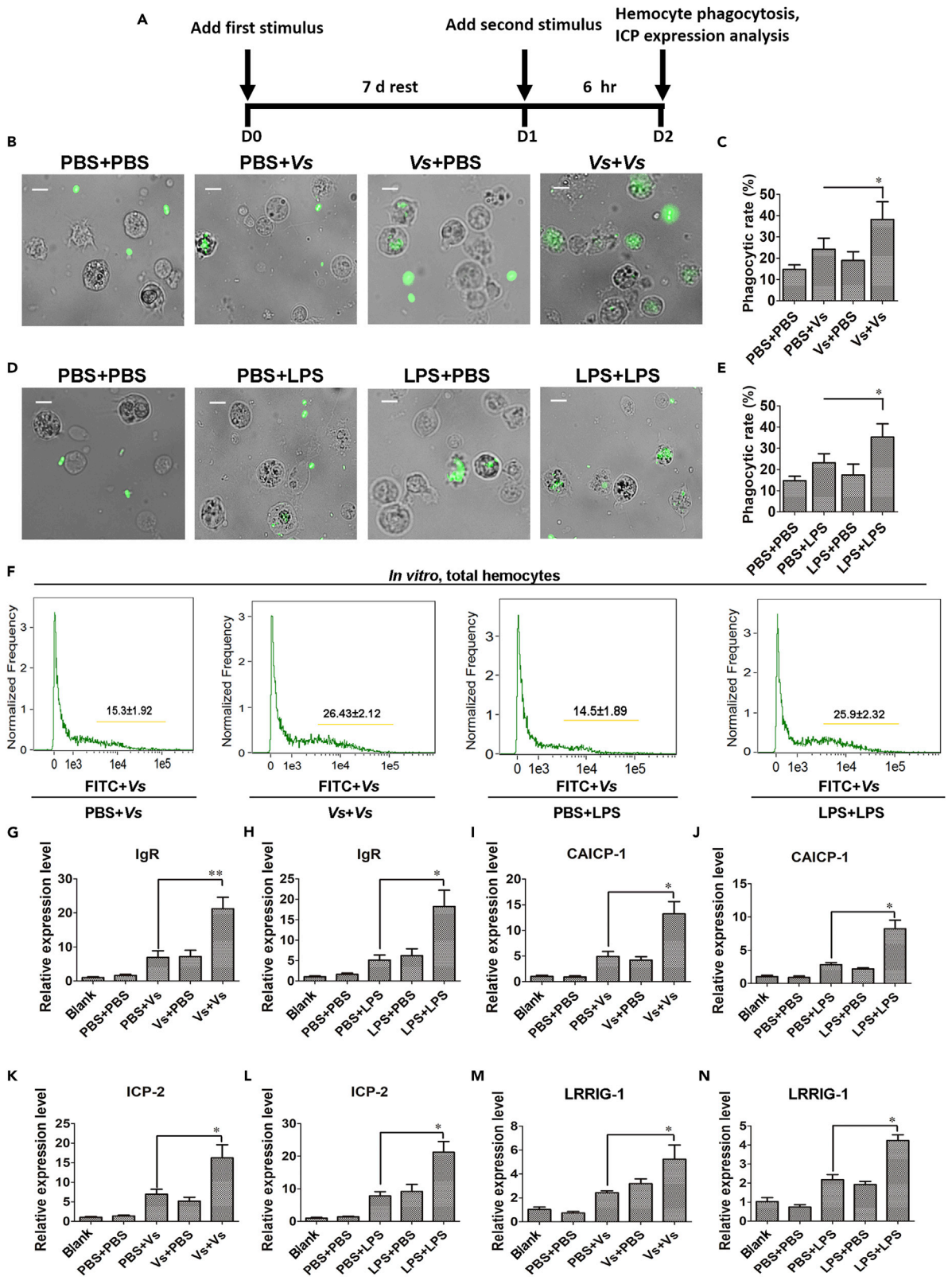
A
Add first stimulus
Add second stimulus
Hemocyte phagocytosis, ICP expression analysis
7 d rest
6 hr
D0
D1
D2
B
PBS+PBS
PBS+Vs
Vs+PBS
Vs+Vs
C
Phagocytic rate (%)
PBS+PBS
PBS+Vs
Vs+PBS
Vs+Vs
D
PBS+PBS
PBS+LPS
LPS+PBS
LPS+LPS
E
Phagocytic rate (%)
PBS+PBS
PBS+LPS
LPS+PBS
LPS+LPS
F
In vitro, total hemocytes
Normalized Frequency
15.3±1.92
FITC+Vs
PBS+Vs
26.43±2.12
FITC+Vs
Vs+Vs
14.5±1.89
FITC+Vs
PBS+LPS
25.9±2.32
FITC+Vs
LPS+LPS
G
IgR
Relative expression level
Blank
PBS+PBS
PBS+Vs
Vs+PBS
Vs+Vs
H
IgR
Relative expression level
Blank
PBS+PBS
PBS+LPS
LPS+PBS
LPS+LPS
I
CAICP-1
Relative expression level
Blank
PBS+PBS
PBS+Vs
Vs+PBS
Vs+Vs
J
CAICP-1
Relative expression level
Blank
PBS+PBS
PBS+LPS
LPS+PBS
LPS+LPS
K
ICP-2
Relative expression level
Blank
PBS+PBS
PBS+Vs
Vs+PBS
Vs+Vs
L
ICP-2
Relative expression level
Blank
PBS+PBS
PBS+LPS
LPS+PBS
LPS+LPS
M
LRRIG-1
Relative expression level
Blank
PBS+PBS
PBS+Vs
Vs+PBS
Vs+Vs
N
LRRIG-1
Relative expression level
Blank
PBS+PBS
PBS+LPS
LPS+PBS
LPS+LPS

Figure 1. Hemocyte Phagocytosis and *Cg*ICPs Participated in Trained Immunity of Oysters

(A) Schematic overview of trained immunity methodology. The oysters were stimulated with *V. splendidus* or LPS. At the eighth day after the first stimulation, the oysters were re-stimulated with *V. splendidus* or LPS for 6 h.

(B–F) Hemocyte phagocytic rates detected by using the immunocytochemistry and flow cytometry in *V. splendidus* or LPS training oysters, respectively. (C) and (E) were the statistical analysis of (B) and (D), respectively. The hemocytes containing labeled bacteria were counted as phagocytosed cells (n = 3). Scale bar: 4 μm.

(G–N) The mRNA transcripts of *Cg*IgR (G), *Cg*CAICP-1 (I), *Cg*ICP-2 (K), and *Cg*LRRIG-1 (M) detected by using qPCR in *V. splendidus* training group (n = 3). The mRNA transcripts of *Cg*IgR (H), *Cg*CAICP-1 (J), *Cg*ICP-2 (L), and *Cg*LRRIG-1 (N) detected by using qPCR in LPS training group (n = 3). Data were representative of three independent experiments and shown as mean ± SD. *: $p < 0.05$, **: $p < 0.01$ (*t* test).

See also Figure S1.

with *V. splendidus* and LPS for immune training and stimulated with *V. splendidus* and LPS again at eighth day after the first stimulation as described above. Hemocytes in *Cg*IgR-RNAi oysters were collected at 6 h after the second stimulation to examine the phagocytic rates and the mRNA transcripts of *Cg*ICPs (Figure 2A). There were no significant changes of hemocyte phagocytic rates toward *V. splendidus* and the mRNA transcripts of *Cg*ICPs (*Cg*IgR, *Cg*CAICP-1, *Cg*ICP-2, *Cg*LRRIG-1) observed in *V. splendidus* and LPS training groups, compared with that in the PBS training group, respectively (Figures 2B–2K).

The Molecular Features of *Cg*IgR and Its Potential Functions in Antibacterial Immunity

In the present study, *Cg*IgR was screened from 190 ICPs in oyster *C. gigas*. There were five extracellular Ig domains, a TM domain, as well as a classical ITAM in its cytoplasmic tail in *Cg*IgR (Figure S2). *Cg*IgR was expressed in all the tested tissues with relatively higher expression level in hemocytes (12.9-fold of that in muscle, $p < 0.05$) (Figure 3A). The mRNA transcripts of *Cg*IgR increased significantly from 6 to 48 h after *V. splendidus* and LPS stimulations and reached the highest level at 12 h (13.1-fold of that in the PBS group, $p < 0.01$) and 24 h (6.13-fold of that in the PBS group, $p < 0.01$) (Figures 3B and 3C), respectively.

The five Ig domains of *Cg*IgR with Trx-his tag (Trx-his-5×Ig) and Trx-his-tag were expressed and purified from *E. coli* (Figure 3D). After the recombinant Trx-his-5×Ig (rTrx-his-5×Ig) was incubated with G^- bacteria (*E. coli* and *V. splendidus*) and G^+ bacteria (*S. aureus* and *M. luteus*), positive bands were revealed by western blotting with anti-His tag mouse monoclonal antibody, whereas no bands were observed in Trx-his tag (control) groups (Figure 3E). The bands for G^- bacteria were obviously thicker than those for G^+ bacteria. The rTrx-his-5×Ig displayed relatively higher binding affinity toward LPS in a dose-dependent manner (Figure 3F), and the maximum binding parameter to bacteria (*B*max) was 0.83 (data not shown).

Western blotting assay of the oyster hemocytes with anti-*Cg*IgR antibody revealed that there was a distinct band of 80 kDa (Figure 3G), indicating the high specificity of anti-*Cg*IgR antibody. There were two bands of 80 and 160 kDa observed in the hemocyte sample by using cross-linking assay with *Cg*IgR antibody after *V. splendidus* stimulation (Figure 3H). There was a distinct band about 80 kDa for r*Cg*IgR revealed by SDS-PAGE assay (Figure 3I), and there was another band about 160 kDa for r*Cg*IgR observed by using native PAGE (Figure 3J). The positive signals of *Cg*IgR were observed in green fluorescence by using anti-*Cg*IgR antibody, which were mainly distributed on the hemocyte membrane. The hemocyte nuclei stained with DAPI were in blue fluorescence (Figure 3K).

After *Cg*IgR was silenced by RNAi, the mRNA expressions of *Cg*ICPs were investigated to reveal the potential immune function of *Cg*IgR. The mRNA transcripts of *Cg*IgR decreased significantly (0.31-fold of that in the EGFP group, $p < 0.05$) after *Cg*IgR was silenced by dsRNA (Figure S3). In *Cg*IgR-RNAi oysters, the mRNA transcripts of *Cg*CAICP-1, *Cg*ICP-2, and *Cg*LRRIG-1 decreased significantly after *V. splendidus* stimulation (0.48-fold, 0.60-fold, and 0.56-fold of that in the EGFP group, $p < 0.05$, respectively) (Figure 3L) and LPS stimulation (0.29-fold, 0.60-fold, and 0.42-fold of that in the EGFP group, $p < 0.05$, respectively) (Figure 3M). Meanwhile, the expressions of *Cg*ICPs were examined after *Cg*IgR was blockaded by using *Cg*IgR antibody. After the injection of *Cg*IgR antibody, the mRNA transcripts of *Cg*CAICP-1, *Cg*ICP-2, and *Cg*LRRIG-1 in *Cg*IgR antibody-blockaded oysters were down-regulated significantly at 6 h after *V. splendidus* stimulation (0.24-fold, $p < 0.01$; 0.63-fold and 0.55-fold, $p < 0.05$) (Figure 3N) and LPS stimulation (0.23-fold, $p < 0.01$; 0.57-fold and 0.55-fold, $p < 0.05$), compared with that in the control group, respectively (Figure 3O).

*Cg*IgR Could Induce *Cg*ICP Production by Interacting with *Cg*Syk after *V. splendidus* and LPS Stimulations

*Cg*Syk was identified from oyster *C. gigas* with two src homology 2 (SH2) domains and a TyrKc domain (Figure 4A). It was expressed in all the tested tissues with relatively higher expressions in gills and hemocytes

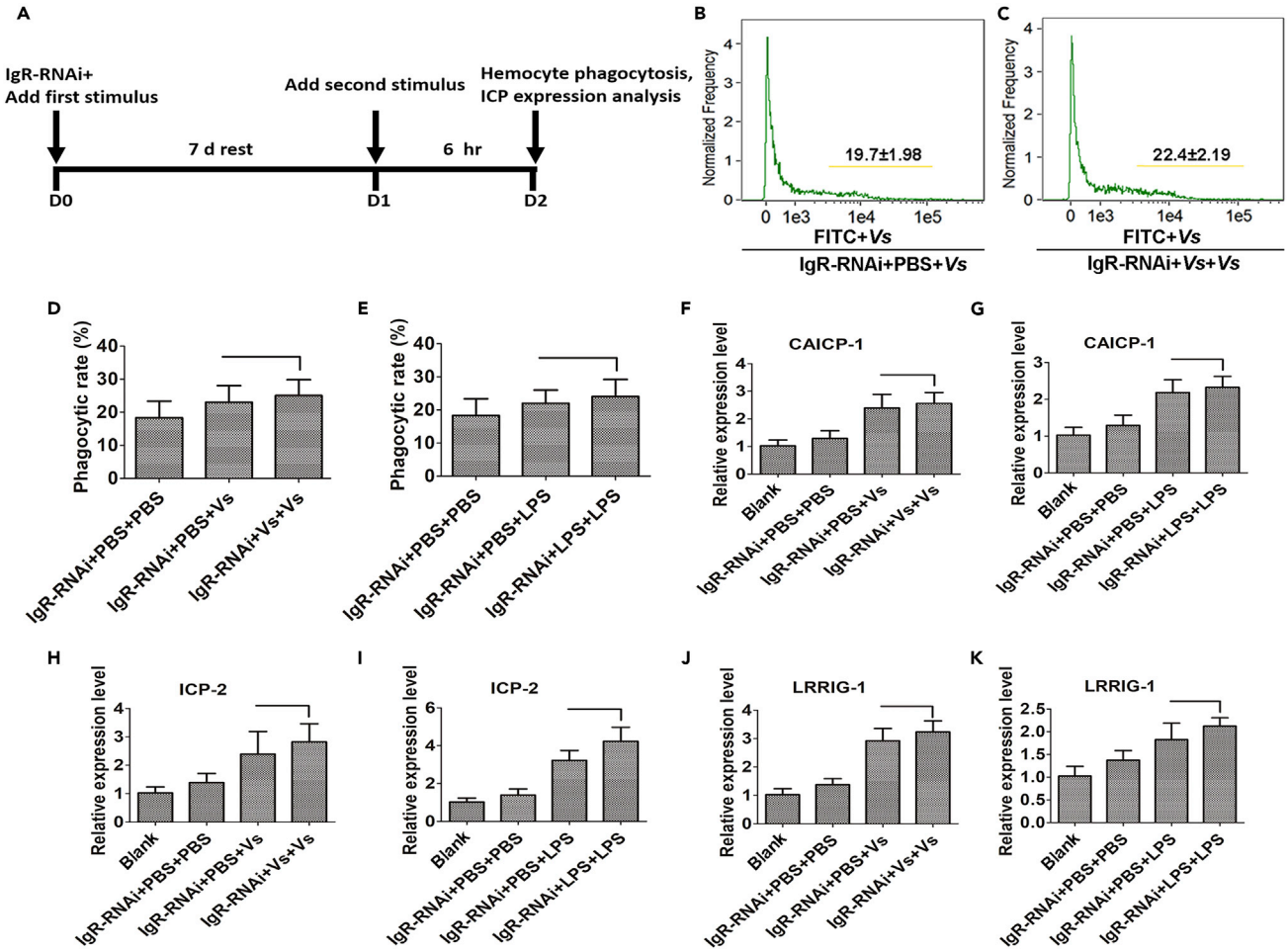

Figure 2. *Cg*IgR Promoted Hemocyte Phagocytosis and *Cg*ICP Production in *V. splendidus* or LPS Immune Training Oysters

(A) Schematic overview of trained immunity methodology in *Cg*IgR-RNAi oysters. *Cg*IgR-RNAi oysters were stimulated with *V. splendidus* or LPS. At the eighth day after the first stimulation, the oysters were re-stimulated with *V. splendidus* or LPS for 6 h.

(B–E) Hemocyte phagocytic rates detected by using the flow cytometry (C) and immunocytochemistry (E) in *Cg*IgR-RNAi oysters after the immune training with *V. splendidus* and LPS (n = 3). (B) and (D) were used as control for (C) and (E), respectively.

(F–K) The mRNA transcripts of *Cg*CAICP-1 (F), *Cg*ICP-2 (H), and *Cg*LRRIG-1 (J) in *Cg*IgR-RNAi oysters detected after the immune training with *V. splendidus*. The mRNA transcripts of *Cg*CAICP-1 (G), *Cg*ICP-2 (I), and *Cg*LRRIG-1 (K) in *Cg*IgR-RNAi oysters detected after the immune training with LPS (n = 3). Data were representative of three independent experiments and shown as mean ± SD.

(3.34-fold and 3.89-fold of that in adductor muscle, $p < 0.05$, respectively) (Figure 4B). The mRNA transcripts of *Cg*Syk in hemocytes increased significantly from 3 to 48 h after *V. splendidus* stimulation and peaked (17.6-fold of that in the PBS group, $p < 0.01$) at 12 h (Figure 4C). After LPS stimulation, *Cg*Syk mRNA transcripts increased significantly from 6 to 48 h and reached the highest level (27.0-fold of that in the PBS group, $p < 0.01$) at 24 h (Figure 4D). The TyrKc domain of *Cg*Syk was expressed and purified from *E. coli* (Figure 4E). Western blotting assay of the hemocyte sample with *Cg*Syk antibody revealed that there was a distinct band of 72 kDa (Figure 4F). After *V. splendidus* and LPS stimulations, the bands of native *Cg*Syk co-immunoprecipitated by *Cg*IgR and *Cg*IgR co-immunoprecipitated by *Cg*Syk both became thicker (Figures 4G and 4H). The expression level of *Cg*Syk was knocked down to 0.39-fold of that in the EGFP group ($p < 0.05$) (Figure S3). In *Cg*Syk-RNAi oysters, the mRNA transcripts of *Cg*CAICP-1, *Cg*ICP-2, and *Cg*LRRIG-1 decreased significantly, which were 0.34-fold ($p < 0.01$), 0.52-fold ($p < 0.05$), and 0.64-fold ($p < 0.05$) after *V. splendidus* stimulation (Figure 4I) and 0.53-fold ($p < 0.05$), 0.40-fold ($p < 0.01$), and 0.42-fold ($p < 0.05$) after LPS stimulation, compared with that in the EGFP group, respectively (Figure 4J). In R406-injected oysters, the mRNA transcripts of *Cg*CAICP-1, *Cg*ICP-2, and *Cg*LRRIG-1 decreased significantly after *V. splendidus* stimulation (0.59-fold, 0.36-fold, and 0.43-fold of that in the DMSO-injected

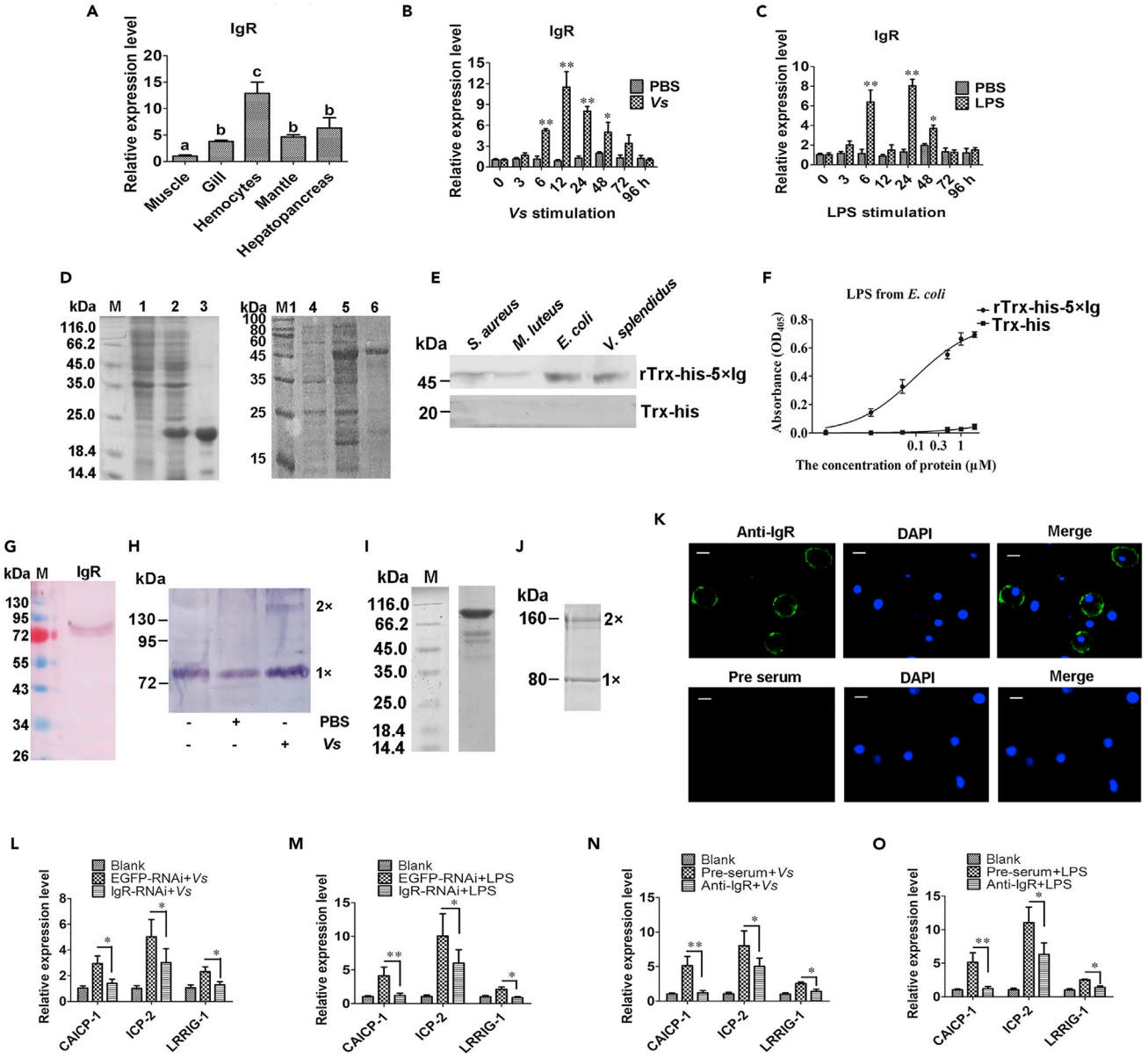

Figure 3. The Potential Functions of *Cg*IgR after *V. splendidus* and LPS Stimulations

(A–C) The tissue distribution of *Cg*IgR (A) and its temporal expression patterns after *V. splendidus* (B) and LPS (C) stimulations (n = 3). PBS was used as control.

(D) The rTrx-his-5×Ig and Trx-his tag (control) expressed and purified from *E. coli*. Lane M, protein marker; Lane 1, rTrx-his-5×Ig and Trx-his tag of *E. coli* with recombinant vectors before induction with IPTG; Lanes 2 and 5, after IPTG induction; Lanes 3 and 6, purified rTrx-his-5×Ig and Trx-his tag.

(E and F) The binding activity of rTrx-his-5×Ig to different bacteria (E) and LPS (F) using anti-His antibody (n = 3).

(G) The molecular mass of native *Cg*IgR detected with polyclonal antibody of anti-*Cg*IgR (n = 3).

(H) Dimer of *Cg*IgR detected with anti-*Cg*IgR antibody *in vivo* treatment of hemocytes after *V. splendidus* stimulation with a cross-linker (BS3) by western blotting (n = 3).

(I and J) Purification of recombinant *Cg*IgR (I) and the native PAGE of r*Cg*IgR (J). Purified r*Cg*IgR was analyzed using native PAGE.

(K) Subcellular localization of *Cg*IgR in hemocytes (n = 3). Scale bar: 5 μm.

(L and M) The mRNA transcripts of *Cg*CAICP-1, *Cg*ICP-2, and *Cg*LRRIG-1 in *Cg*IgR-RNAi oysters detected after *V. splendidus* (L) and LPS (M) stimulations (n = 3).

(N and O) The mRNA transcripts of *Cg*CAICP-1, *Cg*ICP-2, and *Cg*LRRIG-1 in *Cg*IgR antibody-blockaded oysters detected after *V. splendidus* (N) and LPS (O) stimulations (n = 3).

Data were representative of three independent experiments. Error bars represented SD. *: $p < 0.05$, **: $p < 0.01$ (*t* test). Different letters: $p < 0.05$ (one-way ANOVA). See also Figure S2.

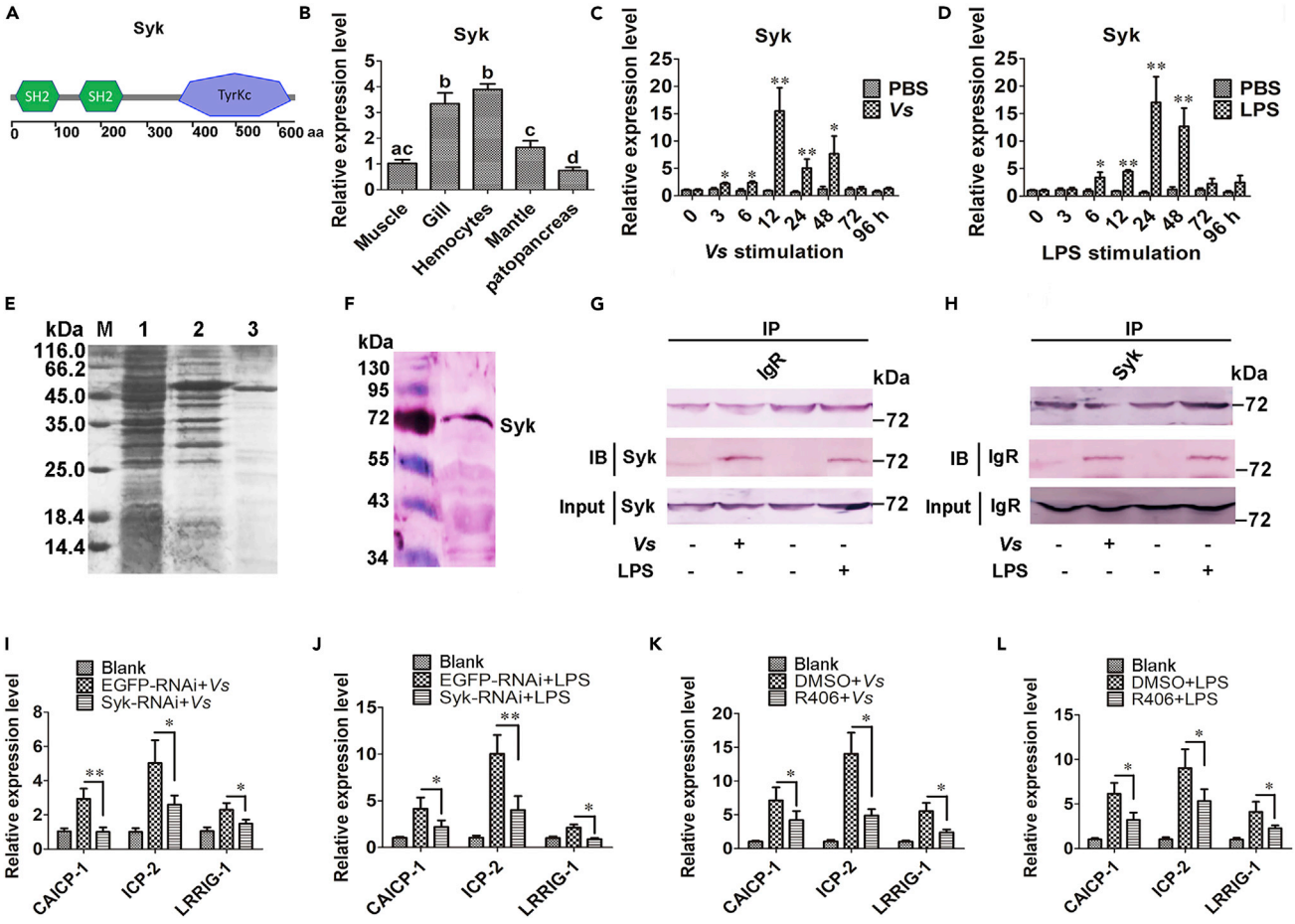

Figure 4. The Potential Functions of *Cg*Syk after *V. splendidus* and LPS Stimulations

(A) The domain architecture of oyster *Cg*Syk.

(B–D) The tissue distribution of *Cg*Syk (B) and its temporal expression patterns after *V. splendidus* (C) and LPS (D) stimulations (n = 3).

(E) The rTyrKc domain of *Cg*Syk was expressed and purified from *E. coli*. Lane M, protein marker; Lane 1, rTyrKc of *E. coli* with recombinant vectors before induction with IPTG; Lane 2, after IPTG induction; Lane 3, purified rTyrKc.

(F) The molecular mass of native *Cg*Syk detected with polyclonal antibody of anti-*Cg*Syk (n = 3).

(G and H) The interaction of *Cg*IgR with *Cg*Syk after *V. splendidus* (G) and LPS (H) stimulations (n = 3).

(I and J) The mRNA transcripts of *Cg*CAICP-1, *Cg*ICP-2, and *Cg*LRRIG-1 in *Cg*Syk-RNAi detected after *V. splendidus* (I) and LPS (J) stimulations (n = 3).

(K and L) The mRNA transcripts of *Cg*CAICP-1, *Cg*ICP-2, and *Cg*LRRIG-1 in R406-injected oysters detected after *V. splendidus* (K) and LPS (L) stimulations (n = 3).

Data were representative of three independent experiments. Error bars represented SD. *: $p < 0.05$, **: $p < 0.01$ (*t* test). Different letters: $p < 0.05$ (one-way ANOVA). See also Figure S3.

group, $p < 0.05$, respectively) (Figure 4K) and LPS stimulation (0.52-fold, 0.59-fold, and 0.55-fold of that in the DMSO-injected group, $p < 0.05$, respectively) (Figure 4L).

IgR/Syk Pathway Induced *Cg*ERK Phosphorylation to Promote the Production of *Cg*ICPs after *V. splendidus* and LPS Stimulations

The phosphorylation of *Cg*ERK was examined to study the involvement of IgR/Syk pathway in regulating *Cg*ICP production. The bands of phospho-*Cg*ERK in *Cg*IgR- and *Cg*Syk-RNAi oysters became thinner, and the count values of these bands decreased significantly after *V. splendidus* (0.24-fold, $p < 0.01$; 0.27-fold, $p < 0.05$) (Figure 5A) and LPS stimulations (0.10-fold and 0.07-fold, $p < 0.001$) (Figure 5B), compared with that in EGFP-RNAi oysters, respectively. After *Cg*IgR was blockaded by anti-*Cg*IgR antibody, the bands of phospho-*Cg*ERK became thinner, and after *V. splendidus* and LPS stimulations, the count values of these bands were 0.17-fold ($p < 0.05$) and 0.12-fold ($p < 0.01$) of that in the pre-serum group, respectively (Figures 5C and 5D). The bands of phospho-*Cg*ERK in R406- and PD98059-injected oysters also became thinner, and the count values of these bands decreased significantly after *V. splendidus* (0.37-fold,

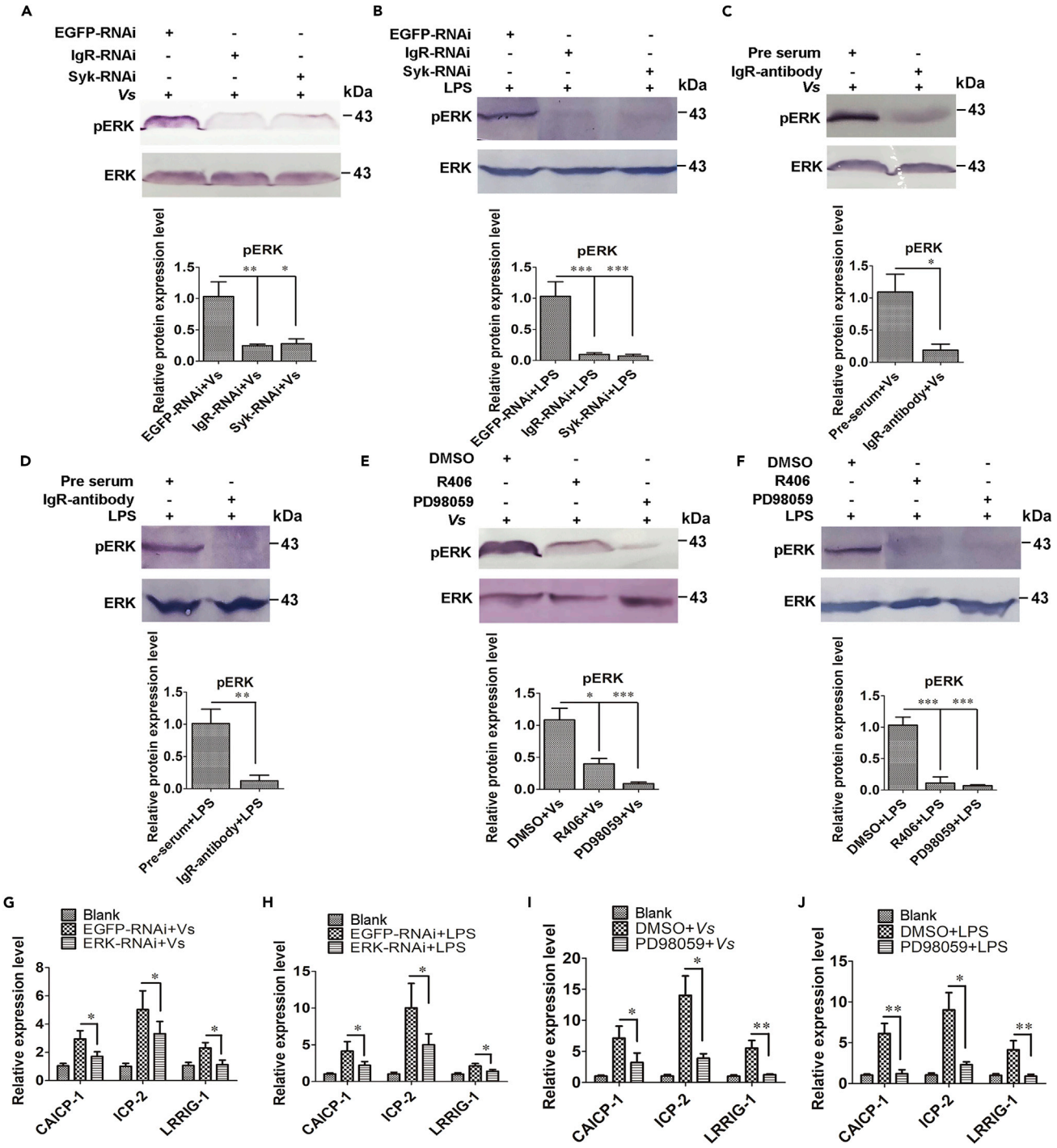

Figure 5. *Cg*IgR-*Cg*Syk Pathway Promoted the Phosphorylation of *Cg*ERK to Induce *Cg*ICP Production

(A) The phospho-*Cg*ERK in *Cg*IgR- or *Cg*Syk-RNAi oysters detected after *V. splendidus* stimulation (n = 3). Histogram was statistical analysis of (A) after digitization with ImageJ.

(B) The phospho-*Cg*ERK in *Cg*IgR- or *Cg*Syk-RNAi oysters detected after LPS stimulation (n = 3). Histogram was statistical analysis of B after digitization with ImageJ.

(C and D) The phospho-*Cg*ERK in *Cg*IgR antibody-blockaded oysters detected after *V. splendidus* and LPS stimulations (n = 3). The statistical analysis of C and D.

(E and F) The phospho-*Cg*ERK in R406- or PD98059-injected oysters detected after *V. splendidus* and LPS stimulations (n = 3). The statistical analysis of E and F.

(G and H) The mRNA transcripts of *Cg*CAICP-1, *Cg*ICP-2, and *Cg*LRRIG-1 in *Cg*ERK-RNAi oysters detected after *V. splendidus* (G) and LPS (H) stimulations (n = 3).

(I and J) The mRNA transcripts of *Cg*CAICP-1, *Cg*ICP-2, and *Cg*LRRIG-1 in PD98059-injected oysters detected after *V. splendidus* (I) and LPS (J) stimulations (n = 3).

Data were representative of three independent experiments. Error bars represented SD. *: $p < 0.05$, **: $p < 0.01$, ***: $p < 0.001$ (*t* test).

p < 0.05; 0.08-fold, p < 0.001) (Figure 5E) and LPS stimulations (0.11-fold and 0.07-fold, p < 0.001), compared with that in the DMSO-injected group, respectively (Figure 5F).

The mRNA transcripts of *Cg*ICPs were assessed by qRT-PCR after *Cg*ERK was knocked down to 0.26-fold of that in the EGFP-RNAi group (p < 0.05) (Figure S3). The mRNA transcripts of *Cg*CAICP-1, *Cg*ICP-2, and *Cg*LRRIG-1 in the *Cg*ERK-RNAi group decreased significantly after *V. splendidus* stimulation (0.57-fold, 0.66-fold, and 0.49-fold, compared with that in the EGFP-RNAi group, respectively, p < 0.05) (Figure 5G) and LPS stimulation (0.53-fold, 0.50-fold, and 0.65-fold, p < 0.05) (Figure 5H). PD98059 was used to inhibit ERK activity, and the mRNA expressions of *Cg*ICPs were examined to evaluate the function of *Cg*ERK in mediating *Cg*ICP production. In PD98059-injected oysters, the mRNA transcripts of *Cg*CAICP-1, *Cg*ICP-2, and *Cg*LRRIG-1 were down-regulated significantly after *V. splendidus* stimulation, which were 0.49-fold, 0.28-fold, and 0.22-fold (p < 0.05) of that in the DMSO-injected group, respectively (Figure 5I). Similarly, the mRNA transcripts of *Cg*CAICP-1, *Cg*ICP-2, and *Cg*LRRIG-1 decreased significantly in PD98059-injected oysters after LPS stimulation, which were 0.20-fold (p < 0.01), 0.26-fold (p < 0.05), and 0.22-fold (p < 0.01) of that in the DMSO-injected group, respectively (Figure 5J).

*Cg*IgR Induced *Cg*H3K4me2 to Promote the Production of *Cg*ICPs after *V. splendidus* and LPS Stimulations

After the oysters were stimulated with *V. splendidus* and LPS, the hemocytes were collected to detect the *Cg*H3K4me2 proteins and the enrichment of *Cg*H3K4me2 on *Cg*ICP promoters. The bands of *Cg*H3K4me2 became thicker and the count values of these bands increased significantly (3.72-fold and 4.50-fold, p < 0.05) after *V. splendidus* and LPS stimulations, compared with that in the PBS group, respectively (Figures 6A and 6B). The values of *Cg*H3K4me2 enrichment on *Cg*ICP-2 (2.92-fold and 3.43-fold, p < 0.05) and *Cg*LRRIG-1 (2.95-fold and 2.70-fold, p < 0.05) promoters increased significantly after *V. splendidus* and LPS stimulations, compared with that in the PBS group, respectively (Figure 6C). The bands of *Cg*H3K4me2 in *Cg*IgR-RNAi oysters became thinner after *V. splendidus* and LPS stimulations, compared with that in the PBS group, respectively (Figures 6D and 6F). The values of *Cg*H3K4me2 enrichment on *Cg*ICP-2 and *Cg*LRRIG-1 promoters decreased significantly after *V. splendidus* stimulation (0.22-fold and 0.45-fold of that in the EGFP-RNAi group, p < 0.05, respectively) (Figure 6E) and LPS stimulation (0.37-fold and 0.36-fold of that in the EGFP-RNAi group, p < 0.05, respectively) (Figure 6G). In *Cg*IgR antibody-blockaded oysters, the bands of *Cg*H3K4me2 became thinner after *V. splendidus* and LPS stimulations, compared with that in the pre-serum group, respectively (Figures 6H and 6J). The enrichment values of *Cg*H3K4me2 on *Cg*ICP-2 and *Cg*LRRIG-1 promoters decreased significantly after *V. splendidus* stimulation (0.42-fold and 0.24-fold, p < 0.05) and LPS stimulation (0.26-fold and 0.29-fold, p < 0.05), compared with that in the pre-serum group, respectively (Figures 6I and 6K).

The Phagocytic Rates of Hemocyte toward *V. splendidus* Decreased Significantly in *Cg*ICP-2- and *Cg*LRRIG-1-RNAi Oysters

After *Cg*ICP-2 and *Cg*LRRIG-1 were knocked down by RNAi, their mRNA transcripts decreased to 0.40-fold and 0.42-fold (p < 0.05) compared with that in the EGFP-RNAi group, respectively (Figure 7A). In *Cg*ICP-2- and *Cg*LRRIG-1-RNAi oysters, the phagocytic rates of hemocytes toward *V. splendidus* were apparently reduced (0.46-fold and 0.59-fold of that in the EGFP-RNAi group, p < 0.05, respectively) (Figures 7B and 7C). The flow cytometry assay also confirmed that the rates of hemocyte phagocytosis toward *V. splendidus* in *Cg*ICP-2- and *Cg*LRRIG-1-RNAi oysters decreased significantly (0.32-fold and 0.44-fold, p < 0.05), compared with that in the EGFP-RNAi group, respectively (Figure 7D). The hemocytes collected from *Cg*ICP-2- and *Cg*LRRIG-1-RNAi oysters were incubated with FITC-labeled *V. splendidus*, and the co-localization of the phagocytized bacteria with lysosomes was detected by immunocytochemical analysis. The FITC-labeled *V. splendidus* was co-localized with lysosomes stained with LysoTracker red and the co-localization signals in *Cg*ICP-2-RNAi and *Cg*LRRIG-1-RNAi oysters were all weakened, compared with that in the EGFP-RNAi group, respectively (Figure 7E).

DISCUSSION

The BCRs, characterized by a complex hetero-oligomeric structure in which ligand binding and signal transduction are compartmentalized into distinct receptor subunits, are essential for the activation of B cells to induce the production of antibodies (Mattila et al., 2013; Yang and Reth, 2010). The BCR/TCR-based adaptive immune strategy is known to have evolved in jawed species and is mediated by B and T cell

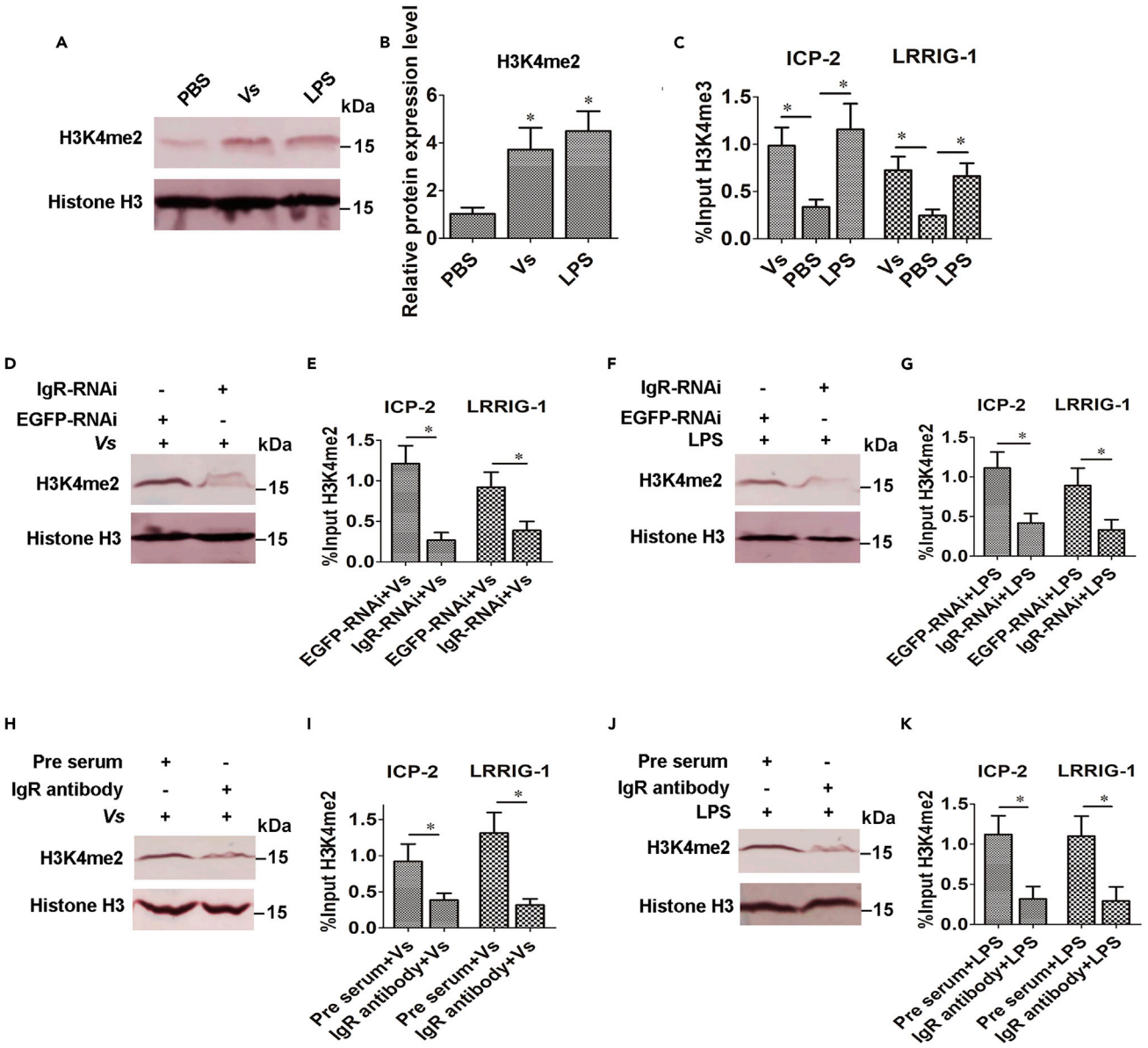

Figure 6. *Cg*IgR Promoted *Cg*H3K4me2 to Induce the mRNA Transcripts of *Cg*ICPs after *V. splendidus* and LPS Stimulations

(A and B) *Cg*H3K4me2 after *V. splendidus* and LPS stimulations (A). (B) was the statistical analysis of *Cg*H3K4me2 after digitization with ImageJ (n = 3).

(C) *Cg*H3K4me2 enrichments for *Cg*ICP-2 and *Cg*LRRIG-1 promoters after *V. splendidus* and LPS stimulations (n = 3).

(D and F) *Cg*H3K4me2 in *Cg*IgR-RNAi oysters after *V. splendidus* (D) and LPS (F) stimulations (n = 3).

(E and G) *Cg*H3K4me2 enrichments on *Cg*ICP-2 and *Cg*LRRIG-1 promoters in *Cg*IgR-RNAi oysters after *V. splendidus* (E) and LPS (G) stimulations (n = 3).

(H and J) *Cg*H3K4me2 in *Cg*IgR-blockage oysters after *V. splendidus* (H) and LPS (J) stimulations (n = 3).

(I and K) The enrichments of *Cg*H3K4me2 on *Cg*ICP-2 and *Cg*LRRIG-1 promoters in *Cg*IgR antibody-blockaded oysters after *V. splendidus* (J) and LPS (K) stimulations (n = 3).

Data were representative of three independent experiments. Error bars represented SD. *: $p < 0.05$ (*t* test).

receptors. Jawless fish (agnathans) represent the most primitive living vertebrates, whereas BCRs and B cells have not been identified in these species (Parra et al., 2013). Although accumulating evidences suggest that invertebrate species could have some memory and specificity in their immune responses, there is still no report about B cells, BCRs, and Igs in invertebrates. In the present study, an ancient BCR-like molecule (defined as *Cg*IgR) was identified from oyster, and its involvement in immune recognition, regulation of *Cg*ICP production, hemocyte phagocytosis, as well as the trained immunity was investigated.

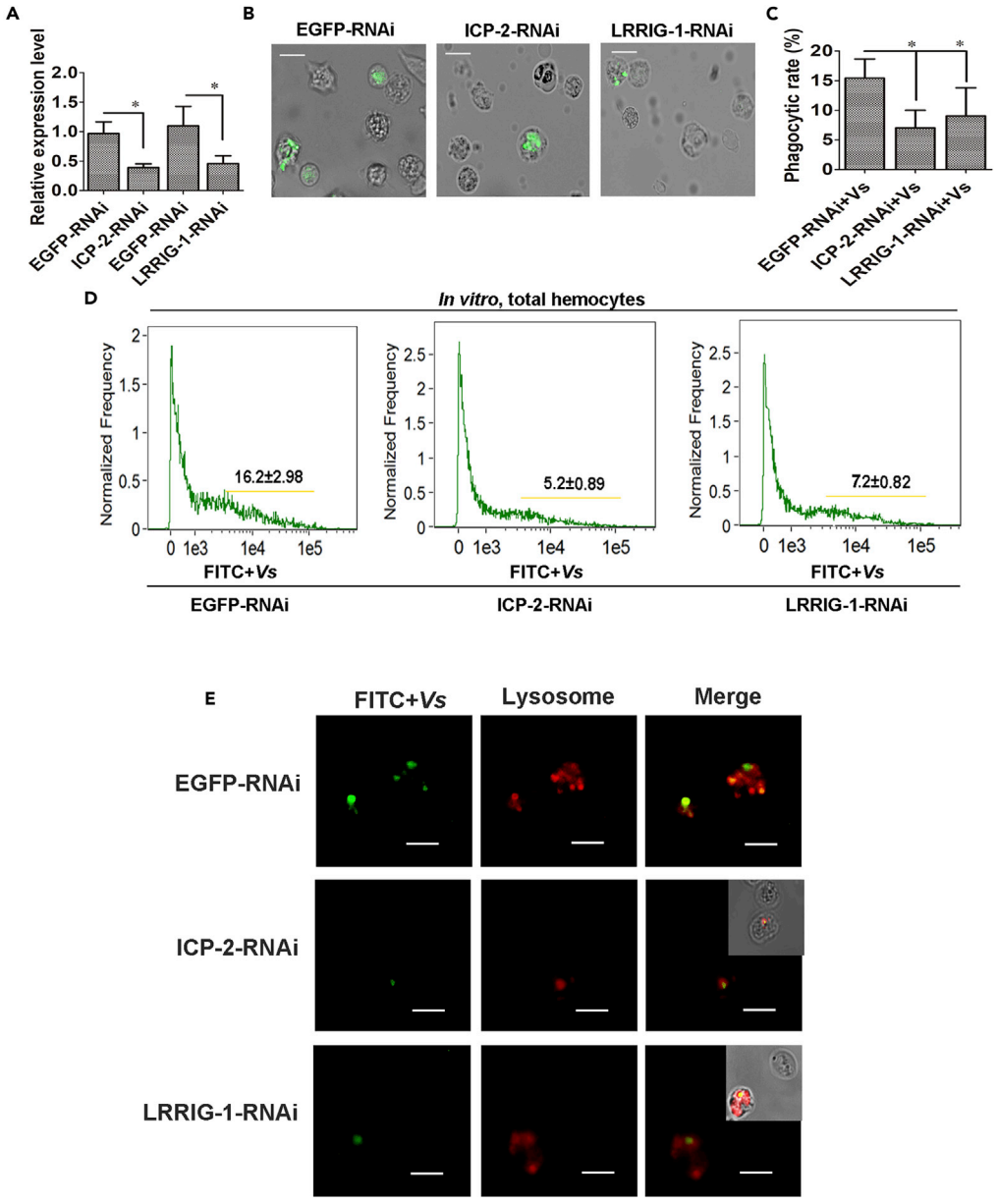

Figure 7. *Cg*ICP-2 and *Cg*LRRIG Promoted Hemocyte Phagocytosis and Degradation toward *V. splendidus*

(A) The mRNA expressions of *Cg*ICP-2- and *Cg*LRRIG-1 in hemocytes after the injection of their specific dsRNA, respectively (n = 3).

(B–D) Hemocyte phagocytic rates toward *V. splendidus* detected by using the immunocytochemistry (B) and flow cytometry (D) in *Cg*ICP-2- or *Cg*LRRIG-1-RNAi oysters (n = 3). (C) was the statistic analysis of (B). EGFP was used as the control. Scale bar: 5 μm.

(E) Co-localization of *V. splendidus* and lysosomes in *Cg*ICP-2- or *Cg*LRRIG-1-RNAi oysters. EGFP was used as the control (n = 3). Scale bar: 5 μm.

Data were representative of three independent experiments. Error bars represented SD. *: $p < 0.05$ (*t* test).

Innate immunity, known as the non-specific immunity or in-born immunity, is an important component of the host defense against a wide variety of pathogens, serving as the front line and providing immediate response in preventing infection. The innate immune responses exhibit memory characteristics after the first encounter with the pathogen (Netea et al., 2016; Saz-Leal et al., 2018; Uehara et al., 2018). For instance, the human monocytes or macrophages exposed continuously to certain pathogen-associated molecular patterns (PAMPs) for a week

displayed strong immune responses to defend against pathogen invasion (Bekkering et al., 2016). This induction of non-specific memory in innate immune cells is termed as trained immunity (Moorlag et al., 2018). As invertebrates lack bona fide B/T cells and antibodies, they depend, to a large extent, on their innate system to recognize and clear invading pathogens. Recently, the trained immunity has also been found in invertebrates. After a primary immunization, mosquito exhibited greater resistance to a subsequent infection with the same pathogen (Simoes and Dimopoulos, 2015). The resistance of brine shrimp *Artemia* against *V. campbellii* invasion was significantly increased when it encountered the homologous bacteria (Norouzitallab et al., 2016). Similarly, in shrimp *Litopenaeus vannamei*, the hemocyte phagocytosis against *V. alginolyticus* was enhanced when the shrimps were re-stimulated with *V. alginolyticus* (Lin et al., 2013). Apart from this, Dscam in *Drosophila* and mosquito also had alternative splicing upon immune stimulus, similar to that of mammalian antibodies (Dong et al., 2006; Hemani and Soller, 2012). In the present study, hemocyte phagocytosis increased significantly in *V. splendidus* and LPS training oysters, which was consistent with the previous reports in oysters (Zhang et al., 2014) and scallops (Wang et al., 2013), indicating the presence of training immunity in mollusks. Ig isotypes have been identified in cartilaginous and teleost fishes (Bengten and Wilson, 2015), whereas there is no report about immunoglobulins in invertebrates to date (Parra et al., 2013). The analysis of transcriptome data indicated that the expression levels of four *Cg*IgCPs (*Cg*IgR, *Cg*CAICP-1, *Cg*ICP-2, *Cg*LRRIG-1) were higher in hemocytes of *V. splendidus* training oysters, compared with that in the PBS training group. Further qRT-PCR analysis also confirmed that the transcripts of *Cg*IgR, *Cg*CAICP-1, *Cg*ICP-2, and *Cg*LRRIG-1 increased significantly in hemocytes of *V. splendidus* training oysters. These results indicated that *Cg*IgR, *Cg*CAICP-1, *Cg*ICP-2, and *Cg*LRRIG-1 were involved in the trained immunity induced by *V. splendidus* or LPS. It was reported that *Cg*CAICP-1 could generate diverse isoforms and mediate hemocyte phagocytosis to different bacteria (Liu et al., 2018). *Cg*LRRIG-1 might function as a PRR to recognize different bacteria and induce the production of tumor necrosis factor 1 (*Cg*TNF-1) and interleukin 17-5 (*Cg*IL17-5) (Wang et al., 2017b). These results suggested that *Cg*IgCPs in oysters might display some similar functions with that of the antibodies in mammals. After *Cg*IgR was knocked down by RNAi, the mRNA transcripts of *Cg*CAICP-1, *Cg*ICP-2, and *Cg*LRRIG-1, as well as hemocyte phagocytosis in *V. splendidus* or LPS training oysters, decreased significantly. These results collectively suggested that *Cg*IgR participated in the trained immunity in oyster by regulating *Cg*IgCP expressions and hemocyte phagocytosis.

The essential component for BCR/TCR-based adaptive immunity, including T cells, B cells, Igs, and major histocompatibility complex (MHC), has been so far identified in cartilaginous and teleost fishes (Bengten and Wilson, 2015). The accumulating evidence indicates that annelids and mollusks have evolved specialized immune cells (Koiwai et al., 2018; Wang et al., 2017a). In most invertebrates, hemocytes play important roles in mediating the immune responses to defend against pathogen invasion, and the granulocytes are the main immunocompetent hemocytes (Christophides et al., 2002; Wang et al., 2017a). The recognition is the key initiation step of the immune response, which is mediated by the PRRs on the surface of immune cells to recognize self and non-self. Some ICPs with TM domain, such as *Es*Dscam in crabs, *Cg*CAICP-1 and *Cg*Siglec-1 in oysters, are found to be highly expressed in hemocytes and function as PRRs to recognize invading bacteria (Li et al., 2018; Liu et al., 2016a, 2018). In the present study, an ancient BCR-like molecule *Cg*IgR was identified from *C. gigas*, which possessed five extracellular Ig domains, a TM domain, and a cytoplasmic tail. The cytoplasmic tail of *Cg*IgR contained a sequence (EGDYTELGQCDPETPYEKL) that was consistent with the classical ITAM sequence (D/ExxYxxL/Ixx(6-12)YxxL/I) in mammalian BCR Igα/Igβ (Monroe, 2006). *Cg*IgR protein was found to be located on the membrane of oyster hemocytes, similar to many other invertebrate ICPs with TM domain (Li et al., 2018; Liu et al., 2016a, 2018). The Ig domain mediates a variety of functions, including pathogen recognition, cell adhesion, and regulation of immune system (Teichmann and Chothia, 2000). Invertebrate ICPs can recognize bacteria and polysaccharides through their Ig domains (Liu et al., 2018). In the present study, the Ig domains of *Cg*IgR displayed binding activities to various bacteria with higher binding activity to G^- bacteria and LPS. These results indicated that the Ig domains could endow *Cg*IgR with recognition and binding activity toward invading bacteria. It was worth noting that *Cg*IgR could form dimers in response against *V. splendidus* stimulation, which was similar to mammalian BCR Igα/Igβ complex. After recognizing antigens, mammalian mIg could interact with BCR Igα/Igβ to form BCR Igα/Igβ complex, which could further transduce signals via their intracellular ITAM (DeFranco, 1993; Monroe, 2006; Reth, 1989), and finally led to the activation of B cells. The recognition capability of extracellular Ig domains and the presence of the classical ITAM in the cytoplasmic tail of *Cg*IgR encouraged us to suspect that invertebrates might have evolved the similar recognition and regulation mechanism of the hemocyte surface receptor as the vertebrate BCRs even if they lacked BCR/TCR-based adaptive immunity.

BCR Igα/Igβ complex occurs through binding of cognate antigen to induce downstream signal transduction, which eventually promotes B cell activation and differentiation (De et al., 2017; Monroe, 2006; Panda and Ding, 2015). Upon ligand binding, the activated BCR Igα/Igβ complex recruits Syk to activate the downstream signaling cascades, including the MEK-ERK1/2 and PLC-NF-κB pathways (Ivashkiv, 2009; Niiro and Clark, 2002; Yang et al., 2015). In invertebrates, the research about ICP functions is mainly focused on cell phagocytosis (Dong et al., 2006; Li et al., 2018; Liu et al., 2018), whereas the signaling mediated by those ICPs has not been reported. In the present study, the activated *Cg*IgR with a classical ITAM in the cytoplasmic tail was found to interact with *Cg*Syk, demonstrating that the signaling mediated by the recognition receptors with ITAM was relatively conserved in vertebrates and invertebrates. In mammals, Syk recruited by the membrane receptors with ITAM participates in the activation of ERK. For example, BCR Igα/Igβ complex and membrane receptor Dectin-1 could recruit Syk to induce ERK phosphorylation (Drummond and Brown, 2013; Monroe, 2006). In the present study, *Cg*IgR was found to interact with *Cg*Syk through its intracellular ITAM to promote *Cg*ERK phosphorylation in oyster, which was similar to BCR Igα/Igβ in inducing Syk-ERK pathway in mammals. These results suggested that there existed an IgR-Syk-ERK signaling pathway in the primitive mollusks, which was similar to BCR Igα/Igβ-mediated Syk-ERK signaling in the mammals.

The activation of BCR Igα/Igβ complex can activate B cells to differentiate into plasmocytes to promote the generation of antibodies in mammals (Mattila et al., 2013; Netea et al., 2016; Yang and Reth, 2010). It has been reported that *Cg*CAICP-1 displays binding activity to different bacteria and functions as an opsonin in mediating hemocyte phagocytosis against bacteria (Liu et al., 2018), and *Cg*LRRIG-1 is also able to recognize various bacteria (Wang et al., 2017b). In the present study, *Cg*IgR could form dimers after recognizing bacteria and activate *Cg*Syk and *Cg*ERK to induce the production of *Cg*ICPs, which might function like mammalian BCR Igα/Igβ complex to transduce signaling to intracellular adaptor to induce the secretions of antibodies (Mattila et al., 2013; Yang and Reth, 2010). All these results suggested that membrane receptor *Cg*IgR in molluscs might be the primitive ancestors of the mammalian BCR Igα/Igβ complex and could activate *Cg*Syk and *Cg*ERK to generate *Cg*ICPs.

The epigenetic modulation is an important characteristic of the immune protection against pathogen infection, and it plays crucial roles in trained immunity. As a kind of epigenetic modification, histone methylation mainly promotes gene transcription through enrichment on gene promoters (Soares et al., 2017). In murine RAW264.7 cells and bone marrow-derived macrophages (BMDMs), H3K4me1, H3K4me2, and H3K4me3 increased after LPS stimulation and the histone methylation in particular H3K4me2 played a critical role in regulating the expressions of IL-6 and TNF-α after LPS stimulation (Zhao et al., 2018). The activated C-type lectin Dectin-1 could promote histone methylation, leading to immune training of monocytes (Quintin et al., 2012) and productions of IL-1β, IL-6, and TNF-α (Saz-Leal et al., 2018). In invertebrates, the study about epigenetic modulation in immunity is still in its infancy, and there is only one report in *Caenorhabditis elegans* about the enhanced monomethylation of Histone H1 variant HIS-24 and the association with daf-21 promoter after *Bacillus thuringiensis* stimulation (Studencka et al., 2012). In the present study, the level of *Cg*H3K4me2 and its enrichment on the promoters of *Cg*ICP-2 and *Cg*LRRIG-1 were found to increase significantly after *V. splendidus* and LPS stimulations. These results indicated that the methylation of *Cg*H3K4 could be induced by *Cg*IgR and participated in the immune response by inducing the expression of *Cg*ICPs in oyster.

Phagocytosis is a major mechanism used to remove pathogens and cell debris, and the phagocytized pathogens are degraded by lysosomes (Krokowski et al., 2018; Li et al., 2016). The phagocytized pathogens form phagosomes in macrophages, and the phagosomes subsequently fuse with intracellular granules to form the phagolysosome. In the phagolysosome, microbial killing is achieved by a combination of non-oxidative and oxidative mechanisms (Pluddemann et al., 2011; Stuart and Ezekowitz, 2005). In the present study, the co-localization of phagocytized *V. splendidus* and lysosomes was observed in hemocytes, which suggested that the phagocytized *V. splendidus* could be degraded by lysosomes in oyster hemocytes. After *Cg*ICP-2 and *Cg*LRRIG-1 were silenced by RNAi, the hemocyte phagocytic rates toward *V. splendidus* were reduced and the co-localization of *V. splendidus* with lysosomes was less observed, indicating that *Cg*ICPs might act as cell surface receptors and opsonins to participate in hemocyte phagocytosis and regulate the degradation of bacteria. The above results demonstrated that *Cg*IgR-mediated signaling could induce the expressions of *Cg*CAICP-1, *Cg*ICP-2, and *Cg*LRRIG-1 to promote the hemocyte phagocytosis and clearance of bacteria, which acted as

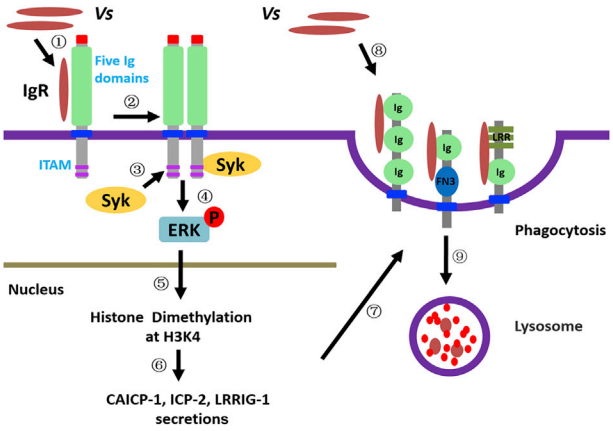

Figure 8. *Cg*IgR-Mediated Pathway Induced *Cg*ICP Production to Promote Hemocyte Phagocytosis and Degradation of *V. splendidus*

Upon recognizing *V. splendidus* and LPS, *Cg*IgR formed dimers and transferred signals to intracellular *Cg*Syk. The activated *Cg*Syk induced *Cg*ERK phosphorylation, which then promoted the enrichments of *Cg*H3K4me2 on *Cg*ICP promoters to induce the production of *Cg*ICPs. *Cg*CAICP-1, *Cg*ICP-2, and *Cg*LRRIG-1 all containing a TM domain could locate on hemocyte membrane to recognize *V. splendidus* and promote hemocyte phagocytosis toward *V. splendidus*, which were then degraded by lysosomes in hemocytes. *Cg*IgR upon recognizing *V. splendidus* and LPS could activate Syk-ERK pathway to induce *Cg*ICP production, which eventually promoted hemocytes to phagocytize and eliminate the invading bacteria.

the similar signaling mediated by BCR Igα/Igβ in promoting antibody secretions to induce bacterial elimination (Niiro and Clark, 2002; Teh and Neuberger, 1997).

In conclusion, an ancient BCR-like molecule *Cg*IgR was identified in oyster *C. gigas*, which was involved in the trained immunity induced by *V. splendidus* and LPS through promoting the transcriptions of *Cg*ICPs and hemocyte phagocytosis. *Cg*IgR with five Ig domains could serve as a hemocyte membrane receptor to recognize different bacteria. The activated *Cg*IgR formed dimers and then interacted with *Cg*Syk through its classical ITAM in cytoplasmic tail. The association of *Cg*IgR with *Cg*Syk could promote *Cg*ERK phosphorylation and induce the dimethylation at *Cg*H3K4, which eventually induced the production of *Cg*CAICP-1, *Cg*ICP-2, and *Cg*LRRIG-1. The produced *Cg*ICPs could initiate the hemocyte phagocytosis toward *V. splendidus*, and the phagocytized *V. splendidus* were finally degraded in hemocyte phagolysosomes (Figure 8). It was suggested that *Cg*IgR in oyster might be one of ancient molecules of mammalian BCR Igα/Igβ complex, and *Cg*IgR-mediated signaling in inducing *Cg*ICP production was similar to that of BCR Igα/Igβ-mediated signaling in promoting antibody secretions. The results demonstrated an ancient BCR-like signaling (*Cg*IgR-mediated signaling) in inducing *Cg*ICP secretions and elucidated the function of *Cg*IgR in trained immunity and the role of *Cg*ICPs in degrading bacteria, indicating the existence, evolution, and functions of ancient BCR-like molecule in molluscs. Although significant disparities are evident between jawed vertebrate immune system and invertebrate immune system, the study of BCR-like signaling will probably unveil the conserved structural and functional aspects of B cell biology among these animals having been subjected to very similar selective pressures.

Limitations of the Study

The study clearly demonstrated an ancient BCR-like signaling (*Cg*IgR-mediated signaling) in inducing *Cg*ICP secretions and the phagocytosis and degradation of bacteria. An ancient BCR-like molecule was identified in oyster, but potential memory cells like B/T cells are still not found in oyster and other invertebrates. *Cg*IgR is defined as one of ancient BCR-like molecules found in oyster, and there might exist other ancient BCR-like molecules in oyster, which still need further investigation in the future. Multiple *Cg*ICPs were found to participate in trained immunity of oyster, and *Cg*IgR could regulate *Cg*ICP secretions and hemocyte phagocytosis in the successive *V. splendidus* and LPS stimulations. However, the involvement of *Cg*IgR-mediated signaling in oyster trained immunity still needs to be further investigated.

METHODS

All methods can be found in the accompanying Transparent Methods supplemental file.

SUPPLEMENTAL INFORMATION

Supplemental Information can be found online at https://doi.org/10.1016/j.isci.2020.100834.

ACKNOWLEDGMENTS

We are grateful to all the laboratory members for their technical advice and helpful discussions. This research was supported by National Key R&D Program (2018YFD0900606), grants (Nos. U1706204, 41961124009) from National Science Foundation of China, Key R&D Program of Liaoning Province (2017203004, 2017203001), earmarked fund (CARS-49) from Modern Agro-industry Technology Research System, the Fund for Outstanding Talents and Innovative Team of Agricultural Scientific Research, AoShan Talents Cultivation Program Supported by Qingdao National Laboratory for Marine Science and Technology (No. 2017ASTCP-OS13), Dalian High Level Talent Innovation Support Program (2015R020), Liaoning Climbing Scholar, the Distinguished Professor of Liaoning, and the Research Foundation for Talented Scholars in Dalian Ocean University.

AUTHOR CONTRIBUTIONS

Study concept and design: J.S., L.W., L.S.; acquisition of data: J.S., L.W., L.S.; analysis and interpretation of data: J.S., L.W., C.Y., L.S.; drafting of the manuscript and preparation of figures: J.S., L.W., L.S.; critical revision of the manuscript: J.S., L.W., L.S.; obtained funding: L.W., L.S.; administrative, technical, or other material support: J.S., L.W., C.Y., L.S.; study supervision: J.S., L.W., L.S.

DECLARATION OF INTERESTS

The authors declare no competing interests.

Received: August 30, 2019
Revised: November 24, 2019
Accepted: January 8, 2020
Published: February 21, 2020

REFERENCES

Bekkering, S., Blok, B.A., Joosten, L.A., Riksen, N.P., van Crevel, R., and Netea, M.G. (2016). In vitro experimental model of trained innate immunity in human primary monocytes. Clin. Vaccine Immunol. *23*, 926–933.

Bengten, E., and Wilson, M. (2015). Antibody repertoires in fish. Results Probl. Cell Differ. *57*, 193–234.

Bonilla, F.A., and Oettgen, H.C. (2010). Adaptive immunity. J. Allergy Clin. Immunol. *125*, S33–S40.

Chang, Y.H., Kumar, R., Ng, T.H., and Wang, H.C. (2018). What vaccination studies tell us about immunological memory within the innate immune system of cultured shrimp and crayfish. Dev. Comp. Immunol. *80*, 53–66.

Christophides, G.K., Zdobnov, E., Barillas-Mury, C., Birney, E., Blandin, S., Blass, C., Brey, P.T., Collins, F.H., Danielli, A., Dimopoulos, G., et al. (2002). Immunity-related genes and gene families in *Anopheles gambiae*. Science *298*, 159–165.

De, S., Zhang, B., Shih, T., Singh, S., Winkler, A., Donnelly, R., and Barnes, B.J. (2017). B cell-intrinsic role for IRF5 in TLR9/BCR-induced human B cell activation, proliferation, and plasmablast differentiation. Front. Immunol. *8*, 1938.

DeFranco, A.L. (1993). Structure and function of the B cell antigen receptor. Annu. Rev. Cell Biol. *9*, 377–410.

Dong, Y., Taylor, H.E., and Dimopoulos, G. (2006). AgDscam, a hypervariable immunoglobulin domain-containing receptor of the *Anopheles gambiae* innate immune system. PLoS Biol. *4*, e229.

Drummond, R.A., and Brown, G.D. (2013). Signalling C-type lectins in antimicrobial immunity. PLoS Pathog. *9*, e1003417.

Hemani, Y., and Soller, M. (2012). Mechanisms of *Drosophila* Dscam mutually exclusive splicing regulation. Biochem. Soc. Trans. *40*, 804–809.

Ivashkiv, L.B. (2009). Cross-regulation of signaling by ITAM-associated receptors. Nat. Immunol. *10*, 340–347.

Jirapongpairoj, W., Hirono, I., and Kondo, H. (2017). Development and evaluation of polyclonal antisera for detection of the IgM heavy chain of multiple fish species. J. Immunol. Methods *449*, 71–75.

Koiwai, K., Kondo, H., and Hirono, I. (2018). The immune functions of sessile hemocytes in three organs of kuruma shrimp *Marsupenaeus japonicus* differ from those of circulating hemocytes. Fish Shellfish Immunol. *78*, 109–113.

Konigsberger, S., Prodohl, J., Stegner, D., Weis, V., Andreas, M., Stehling, M., Schumacher, T., Bohmer, R., Thielmann, I., van Eeuwijk, J.M., et al. (2012). Altered BCR signalling quality predisposes to autoimmune disease and a pre-diabetic state. EMBO J. *31*, 3363–3374.

Krokowski, S., Lobato-Marquez, D., Chastanet, A., Pereira, P.M., Angelis, D., Galea, D., Larrouy-Maumus, G., Henriques, R., Spiliotis, E.T., Carballido-Lopez, R., et al. (2018). Septins recognize and entrap dividing bacterial cells for delivery to lysosomes. Cell Host Microbe *24*, 866–874.e4.

Kurtz, J., and Armitage, S.A. (2006). Alternative adaptive immunity in invertebrates. Trends Immunol. *27*, 493–496.

Kwak, K., Akkaya, M., and Pierce, S.K. (2019). B cell signaling in context. Nat. Immunol. *20*, 963–969.

Lau, Y.T., Sussman, L., Pales Espinosa, E., Katalay, S., and Allam, B. (2017). Characterization of hemocytes from different body fluids of the eastern oyster *Crassostrea virginica*. Fish Shellfish Immunol. *71*, 372–379.

Li, X., He, S., Zhou, X., Ye, Y., Tan, S., Zhang, S., Li, R., Yu, M., Jundt, M.C., Hidebrand, A., et al. (2016). Lyn delivers bacteria to lysosomes for eradication through TLR2-initiated autophagy related phagocytosis. PLoS Pathog. *12*, e1005363.

Li, X.J., Yang, L., Li, D., Zhu, Y.T., Wang, Q., and Li, W.W. (2018). Pathogen-specific binding soluble Down syndrome cell adhesion molecule (Dscam) regulates phagocytosis via membrane-bound Dscam in crab. Front. Immunol. *9*, 801.

Lin, Y.C., Chen, J.C., Morni, W.Z., Putra, D.F., Huang, C.L., Li, C.C., and Hsieh, J.F. (2013). Vaccination enhances early immune responses in white shrimp *Litopenaeus vannamei* after secondary exposure to *Vibrio alginolyticus*. PLoS One *8*, e69722.

Liu, C., Jiang, S., Wang, M., Wang, L., Chen, H., Xu, J., Lv, Z., and Song, L. (2016a). A novel siglec (CgSiglec-1) from the Pacific oyster (*Crassostrea gigas*) with broad recognition spectrum and inhibitory activity to apoptosis, phagocytosis and cytokine release. Dev. Comp. Immunol. *61*, 136–144.

Liu, C., Wang, M., Jiang, S., Wang, L., Chen, H., Liu, Z., Qiu, L., and Song, L. (2016b). A novel junctional adhesion molecule A (CgJAM-A-L) from oyster (*Crassostrea gigas*) functions as pattern recognition receptor and opsonin. Dev. Comp. Immunol. *55*, 211–220.

Liu, D., Yi, Q., Wu, Y., Lu, G., Gong, C., Song, X., Sun, J., Qu, C., Liu, C., Wang, L., et al. (2018). A hypervariable immunoglobulin superfamily member from *Crassostrea gigas* functions as pattern recognition receptor with opsonic activity. Dev. Comp. Immunol. *86*, 96–108.

Mattila, P.K., Feest, C., Depoil, D., Treanor, B., Montaner, B., Otipoby, K.L., Carter, R., Justement, L.B., Bruckbauer, A., and Batista, F.D. (2013). The actin and tetraspanin networks organize receptor nanoclusters to regulate B cell receptor-mediated signaling. Immunity *38*, 461–474.

Monroe, J.G. (2006). ITAM-mediated tonic signalling through pre-BCR and BCR complexes. Nat. Rev. Immunol. *6*, 283–294.

Moorlag, S., Roring, R.J., Joosten, L.A.B., and Netea, M.G. (2018). The role of the interleukin-1 family in trained immunity. Immunol. Rev. *281*, 28–39.

Moreau, P., Moreau, K., Segarra, A., Tourbiez, D., Travers, M.A., Rubinsztein, D.C., and Renault, T. (2015). Autophagy plays an important role in protecting Pacific oysters from OsHV-1 and *Vibrio aestuarianus* infections. Autophagy *11*, 516–526.

Netea, M.G., Joosten, L.A., Latz, E., Mills, K.H., Natoli, G., Stunnenberg, H.G., O'Neill, L.A., and Xavier, R.J. (2016). Trained immunity: a program of innate immune memory in health and disease. Science *352*, aaf1098.

Netea, M.G., Quintin, J., and van der Meer, J.W. (2011). Trained immunity: a memory for innate host defense. Cell Host Microbe *9*, 355–361.

Niiro, H., and Clark, E.A. (2002). Regulation of B-cell fate by antigen-receptor signals. Nat. Rev. Immunol. *2*, 945–956.

Norouzitallab, P., Baruah, K., Biswas, P., Vanrompay, D., and Bossier, P. (2016). Probing the phenomenon of trained immunity in invertebrates during a transgenerational study, using brine shrimp Artemia as a model system. Sci. Rep. *6*, 21166.

Ollila, J., and Vihinen, M. (2005). B cells. Int. J. Biochem. Cell Biol. *37*, 518–523.

Panda, S., and Ding, J.L. (2015). Natural antibodies bridge innate and adaptive immunity. J. Immunol. *194*, 13–20.

Papavasiliou, F., Jankovic, M., Suh, H., and Nussenzweig, M.C. (1995). The cytoplasmic domains of immunoglobulin (Ig) alpha and Ig beta can independently induce the precursor B cell transition and allelic exclusion. J. Exp. Med. *182*, 1389–1394.

Parra, D., Takizawa, F., and Sunyer, J.O. (2013). Evolution of B cell immunity. Annu. Rev. Anim. Biosci. *1*, 65–97.

Pluddemann, A., Mukhopadhyay, S., and Gordon, S. (2011). Innate immunity to intracellular pathogens: macrophage receptors and responses to microbial entry. Immunol. Rev. *240*, 11–24.

Quintin, J., Saeed, S., Martens, J.H.A., Giamarellos-Bourboulis, E.J., Ifrim, D.C., Logie, C., Jacobs, L., Jansen, T., Kullberg, B.J., Wijmenga, C., et al. (2012). *Candida albicans* infection affords protection against reinfection via functional reprogramming of monocytes. Cell Host Microbe *12*, 223–232.

Reth, M. (1989). Antigen receptor tail clue. Nature *338*, 383–384.

Rolli, V., Gallwitz, M., Wossning, T., Flemming, A., Schamel, W.W., Zurn, C., and Reth, M. (2002). Amplification of B cell antigen receptor signaling by a Syk/ITAM positive feedback loop. Mol. Cell *10*, 1057–1069.

Rowley, R.B., Burkhardt, A.L., Chao, H.G., Matsueda, G.R., and Bolen, J.B. (1995). Syk protein-tyrosine kinase is regulated by tyrosine-phosphorylated Ig alpha/Ig beta immunoreceptor tyrosine activation motif binding and autophosphorylation. J. Biol. Chem. *270*, 11590–11594.

Saz-Leal, P., Del Fresno, C., Brandi, P., Martinez-Cano, S., Dungan, O.M., Chisholm, J.D., Kerr, W.G., and Sancho, D. (2018). Targeting SHIP-1 in myeloid cells enhances trained immunity and boosts response to infection. Cell Rep. *25*, 1118–1126.

Simoes, M.L., and Dimopoulos, G. (2015). A mosquito mediator of parasite-induced immune priming. Trends Parasitol. *31*, 402–404.

Simon, R., Diaz-Rosales, P., Morel, E., Martin, D., Granja, A.G., and Tafalla, C. (2019). CpG oligodeoxynucleotides modulate innate and adaptive functions of IgM(+) B cells in *rainbow trout*. Front. Immunol. *10*, 584.

Smith, N.C., Rise, M.L., and Christian, S.L. (2019). A comparison of the innate and adaptive immune systems in cartilaginous fish, ray-finned fish, and lobe-finned fish. Front. Immunol. *10*, 2292.

Soares, L.M., He, P.C., Chun, Y., Suh, H., Kim, T., and Buratowski, S. (2017). Determinants of histone H3K4 methylation patterns. Mol. Cell *68*, 773–785.e6.

Stuart, L.M., and Ezekowitz, R.A. (2005). Phagocytosis: elegant complexity. Immunity *22*, 539–550.

Studencka, M., Konzer, A., Moneron, G., Wenzel, D., Opitz, L., Salinas-Riester, G., Bedet, C., Kruger, M., Hell, S.W., Wisniewski, J.R., et al. (2012). Novel roles of *Caenorhabditis elegans* heterochromatin protein HP1 and linker histone in the regulation of innate immune gene expression. Mol. Cell. Biol. *32*, 251–265.

Teh, Y.M., and Neuberger, M.S. (1997). The immunoglobulin (Ig)alpha and Igbeta cytoplasmic domains are independently sufficient to signal B cell maturation and activation in transgenic mice. J. Exp. Med. *185*, 1753–1758.

Teichmann, S.A., and Chothia, C. (2000). Immunoglobulin superfamily proteins in *Caenorhabditis elegans*. J. Mol. Biol. *296*, 1367–1383.

Torre, C., Laure Tsoumtsa, L., and Ghigo, E. (2017). Trained immunity in invertebrates: what do we know? Med. Sci. (Paris) *33*, 979–983.

Uehara, H., Minami, K., Quante, M., Nian, Y., Heinbokel, T., Azuma, H., Khal, A.E., and Tullius, S.G. (2018). Recall features and allorecognition in innate immunity. Transpl. Int. *31*, 6–13.

Wang, J., Wang, L., Yang, C., Jiang, Q., Zhang, H., Yue, F., Huang, M., Sun, Z., and Song, L. (2013). The response of mRNA expression upon secondary challenge with Vibrio anguillarum suggests the involvement of C-lectins in the immune priming of scallop *Chlamys farreri*. Dev. Comp. Immunol. *40*, 142–147.

Wang, W., Li, M., Wang, L., Chen, H., Liu, Z., Jia, Z., Qiu, L., and Song, L. (2017a). The granulocytes are the main immunocompetent hemocytes in *Crassostrea gigas*. Dev. Comp. Immunol. *67*, 221–228.

Wang, W., Song, X., Wang, L., and Song, L. (2018b). Pathogen-derived carbohydrate recognition in molluscs immune defense. Int. J. Mol. Sci. *19*, 721.

Wang, X., Wang, M., Xu, Q., Xu, J., Lv, Z., Wang, L., and Song, L. (2017b). Two novel LRR and Ig domain-containing proteins from oyster *Crassostrea gigas* function as pattern recognition receptors and induce expression of cytokines. Fish Shellfish Immunol. *70*, 308–318.

Wang, L., Song, X., and Song, L. (2018a). The oyster immunity. Dev. Comp. Immunol. *80*, 99–118.

Werner, M., Hobeika, E., and Jumaa, H. (2010). Role of PI3K in the generation and survival of B cells. Immunol. Rev. *237*, 55–71.

Yang, J., and Reth, M. (2010). The dissociation activation model of B cell antigen receptor triggering. FEBS Lett. *584*, 4872–4877.

Yang, S.F., Zhuang, T.F., Si, Y.M., Qi, K.Y., and Zhao, J. (2015). *Coriolus versicolor* mushroom polysaccharides exert immunoregulatory

effects on mouse B cells via membrane Ig and TLR-4 to activate the MAPK and NF-kappaB signaling pathways. Mol. Immunol. *64*, 144–151.

Yu, Y.Y., Kong, W., Yin, Y.X., Dong, F., Huang, Z.Y., Yin, G.M., Dong, S., Salinas, I., Zhang, Y.A., and Xu, Z. (2018). Mucosal immunoglobulins protect the olfactory organ of teleost fish against parasitic infection. PLoS Pathog. *14*, e1007251.

Zhang, G., Fang, X., Guo, X., Li, L., Luo, R., Xu, F., Yang, P., Zhang, L., Wang, X., Qi, H., et al. (2012). The oyster genome reveals stress adaptation and complexity of shell formation. Nature *490*, 49–54.

Zhang, T., Qiu, L., Sun, Z., Wang, L., Zhou, Z., Liu, R., Yue, F., Sun, R., and Song, L. (2014). The specifically enhanced cellular immune responses in Pacific oyster (*Crassostrea gigas*) against secondary challenge with *Vibrio splendidus*. Dev. Comp. Immunol. *45*, 141–150.

Zhang, L., Li, L., Guo, X., Litman, G.W., Dishaw, L.J., and Zhang, G. (2015). Massive expansion and functional divergence of innate immune genes in a protostome. Sci. Rep. *5*, 8693.

Zhao, S., Zhong, Y., Fu, X., Wang, Y., Ye, P., Cai, J., Liu, Y., Sun, J., Mei, Z., Jiang, Y., et al. (2018). H3K4 methylation regulates LPS-induced proinflammatory cytokine expression and release in macrophages. Shock *51*, 401–406.

iScience, Volume *23*

Supplemental Information

An Ancient BCR-like Signaling Promotes ICP Production and Hemocyte Phagocytosis in Oyster

Jiejie Sun, Lingling Wang, Chuanyan Yang, and Linsheng Song

An ancient BCR-like signaling promotes ICP production and hemocyte phagocytosis in oyster

Jiejie Sun[a,c], Lingling Wang[a,b,c,d*], Chuanyan Yang[a,c], Linsheng Song[a,b,c,e*]

[a] Liaoning Key Laboratory of Marine Animal Immunology, Dalian Ocean University, Dalian 116023, China

[b] Laboratory of Marine Fisheries Science and Food Production Processes, Qingdao National Laboratory for Marine Science and Technology, Qingdao 266235, China

[c] Liaoning Key Laboratory of Marine Animal Immunology & Disease Control, Dalian Ocean University, Dalian 116023, China

[d] Dalian Key Laboratory of Aquatic Animal Diseases Prevention and Control, Dalian Ocean University, Dalian 116023, China

[e] Lead Contact

*Corresponding to:

Prof. Lingling Wang, Linsheng Song

Dalian Ocean University

52 Heishijiao Street, Dalian 116023, China

Tel: 86-411-84763173

E-mail: wanglingling@dlou.edu.cn (L. Wang); lshsong@dlou.edu.cn (L. Song).

Supplementary information

Supplemental Figures and Figure legends

Figure S1.

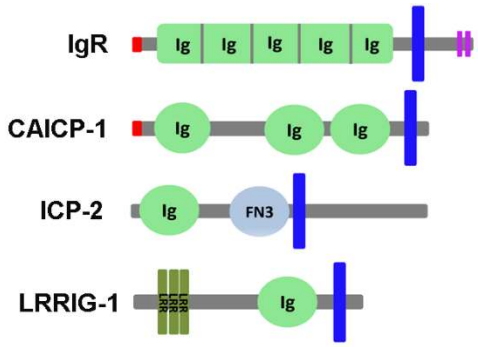

Figure S1. Schematic representations of *Cg*ICPs indicating different domains, Related to Figure 1. *Cg*IgR contained a signal peptide (SP), five immunoglobulin (Ig) domains, a transmembrane (TM) domain and cytoplasmic tail with a classical ITAM. *Cg*CAICP-1 contained a SP, three Ig domains and a TM domain. *Cg*ICP-2 contained an Ig domain, a fibronectin type 3 (FN3) domain, a TM domain and cytoplasmic tail. *Cg*LRRIG-1 contained three leucine-rich repeat (LRR) domains, an Ig domain and a TM domain.

Figure S2.

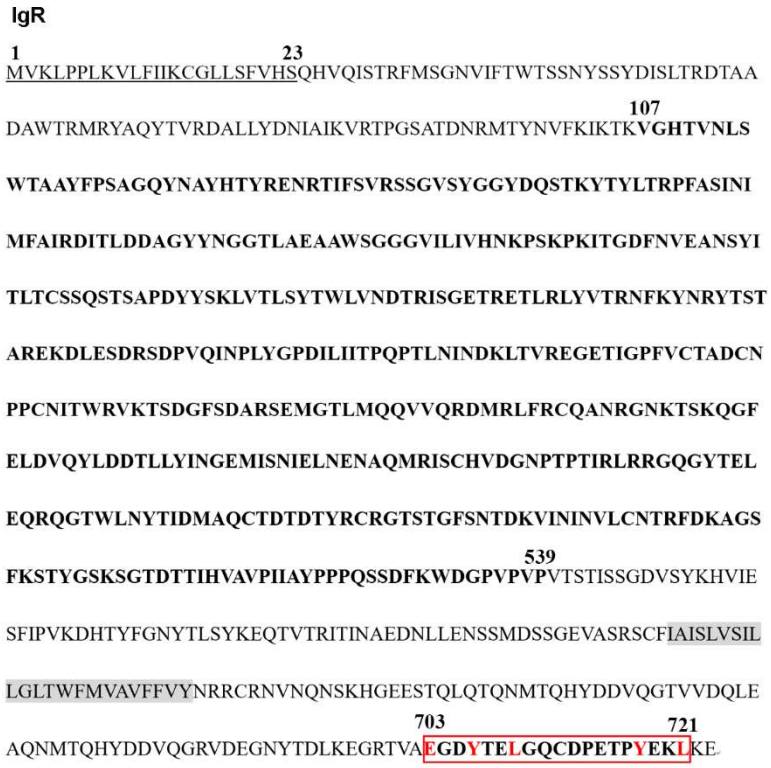

Figure S2. The protein sequence of *Cg*IgR, Related to Figure 3. The sequence was subjected to online SMART analysis. The amino acids were numbered. The signal peptide was underlined, five Ig domains were bolded, a TM domain was shadowed and the classical ITAM in cytoplasm tail was boxed with red.

Figure S3.

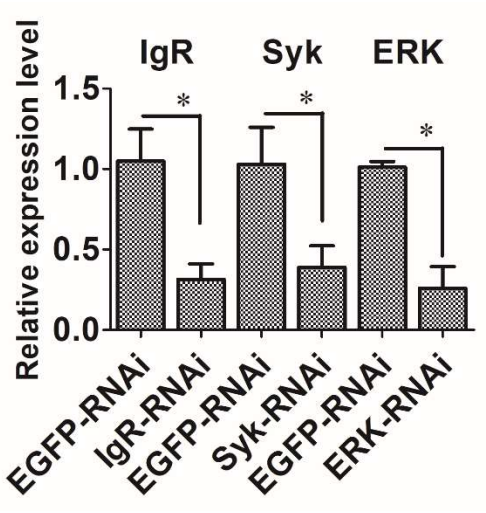

Figure S3. RNAi efficiencies of *Cg*IgR, *Cg*Syk and *Cg*ERK were analyzed by qRT-PCR (n=3), Related to Figure 4. EGFP-RNAi group was used as control. Data were representative of three independent experiments. Error bars represented SD. *$p < 0.05$, **$p < 0.01$ (*t*-test).

Supplemental Table

Table S1. Sequences of the primers used in this study, related to Figure 1 to Figure 7.

Primer	Sequence (5'-3')
Clone primers	
*Cg*IgR-F	ACCTACACTGTTATAGCAG
*Cg*IgR-R	ACGAGAAGTTAAAGGAATGA
*Cg*ERK-F	CGAGCTCTCTATCAAC
*Cg*ERK-R	TTATAAATCAGCAATTCC
Recombinant expression	
*Cg*IgR-ExF	TACTCAGGATCCAGAATGACATACAATGTCTTC
*Cg*IgR-ExR	TACTCACTCGAGTGTGTTGCTGAATCCTGTAG
*Cg*Syk-ExF	TACTCAGGATCCATGAAGATTTATGACACT
*Cg*Syk-ExR	TACTCACTCGAGACTCATCTTGGTCTCTAG
RT-PCR primers	
*Cg*IgR-RT-F	ACAATCAACGCTGAAGATAACCT
*Cg*IgR-RT-R	AAACACTGCCACCATAAACCAC
*Cg*Syk-RT-F	GCGTAATGTACTGCTGGTGGA
*Cg*Syk-RT-R	TCATCAGGACAACGAGGTGG
*Cg*ERK-RT-F	ATCGTGACCTCAAGCCCA
*Cg*ERK-RT-R	TGCCAGGATACAGCCAACA
*Cg*CAICP-1-RT-F	ATAGTCCTTGTCATCCTCGTTATC
*Cg*CAICP-1-RT-R	TTCGTTCTCAGAGTCGTGTCCAGT
*Cg*ICP-2-RT-F	CTATTTGCTGGATTCCTGGC
*Cg*ICP-2-RT-R	GTTCTTCATTTGTATTAGCGTCG
*Cg*LRRIG-1-RT-F	TCACTGTGGCAGTGGTAGTGTGC
*Cg*LRRIG-1-RT-R	TCGGACCGTTTCGGAAAGGCA
*Cg*EF-RT-F	AGTCACCAAGGCTGCACAGAAAG
*Cg*EF-RT-R	TCCGACGTATTTCTTTGCGATGT
RNA interference	
*Cg*IgR-Fi	GCGTAATACGACTCACTATAGGCACGTGATCGAAAGCTTCATC
*Cg*IgR-Ri	GCGTAATACGACTCACTATAGGGTATGTCACGTATGTAACCTTC
*Cg*Syk-Fi	GCGTAATACGACTCACTATAGGGAGATCATGTGGCAAGTCG
*Cg*Syk-Ri	GCGTAATACGACTCACTATAGGATAGCAATGTCCTGATGGGTG
*Cg*ERK-Fi	GCGTAATACGACTCACTATAGGTTGGCTCGAGTAGCTGAC
*Cg*ERK-Ri	GCGTAATACGACTCACTATAGGTTATAAATCAGCAATTCC
*Cg*ICP-2-Fi	GCGTAATACGACTCACTATAGGACCTGATGTAGTATTGTACGC
*Cg*ICP-2-Ri	GCGTAATACGACTCACTATAGGTAACTGGAAAAAAGATAATTG
*Cg*LRRIG-1-Fi	GCGTAATACGACTCACTATAGGCTGTGTACCAGCATCTGTA
*Cg*LRRIG-1-Ri	GCGTAATACGACTCACTATAGGGCATGATCACCTTCGAAT
EGFP-Fi	GCGTAATACGACTCACTATAGGTGGTCCCAATTCTCGTGGAAC
EGFP-Ri	GCGTAATACGACTCACTATAGGCTTGAAGTTGACCTTGATGCC
Promoters	
*Cg*ICP-2-proF	TAAGGGAAGGGGAGACTATTGG
*Cg*ICP-2-proR	CAGAACGAGCATCGCTGAATC
*Cg*LRRIG-proF	AACATCAGTAGACTTATGCCGCC
*Cg*LRRIG-proF	CTGTTCTAAGAGCCGCTGTTCA

Transparent methods

Oysters and cultivation

Pacific oysters, *C. gigas* (shell length 12-16 cm each), purchased from a local farm in Dalian, Liaoning, China, were cultured in aerated seawater at 15 ± 2°C for one week. The food of powdered algae (commercially purchased) was added to the water every other day. The seawater in the aquaria was replaced every day.

cDNA cloning and sequence analysis

The sequence information of *Cg*IgR (XM_011422710.2) was acquired from NCBI database (https://www.ncbi.nlm.nih.gov/) and the primers of *Cg*IgR (Table 1) were designed to clone the full-length sequence of *Cg*IgR. A translation tool (http://web.expasy.org/translate/) was used to predict the amino acid sequence and Swiss model (https://swissmodel.expasy.org) were used to predict protein domains of *Cg*IgR.

Immune challenge and sample collection

A total of 240 oysters were employed and randomly divided into three groups, control group, LPS group, and *V. splendidus* group. The oysters in the three groups individually received an injection with 100 μL of 0.5 mg mL^{-1} phosphate-buffered saline (PBS) (0.14 M NaCl, 2.7 mM KCl, 10 mM Na_2HPO_4, and 1.8 mM KH_2PO_4), 100 μL of *V. splendidus* (10^6 CFU mL^{-1}) and 100 μL of LPS (0.5 mg mL^{-1}) from *Escherichia coli* (O222:B44, Sigma) dissolved in PBS, respectively. Nine oysters were randomly sampled from each group and the hemolymphs were collected at 0, 3, 6, 12, 24, 48, 72 and 96 h after injection with PBS, LPS and *V.*

splendidus, respectively. The hemolymphs collected from three oysters were pooled together as one sample, and there were three samples for each time point. The hemocytes were harvested by centrifugation at 800 *g*, 4°C for 10 min. The total RNA was extracted from the collected hemocytes to detect the temporal expression patterns of *Cg*IgR and *Cg*Syk (XM_011448334.2).

Different tissues (hemocytes, adductor muscle, gills, mantle and hepatopancreas) were collected from nine untreated oysters for RNA extraction using Trizol reagent (Invitrogen) to examine the distributions of *Cg*IgR and *Cg*Syk mRNAs in different tissues.

Quantitative real-time PCR (qRT-PCR) analysis

qRT-PCR was performed to detect the tissue distribution of *Cg*IgR and *Cg*Syk mRNAs by using primers *Cg*IgR-RT-F and -RT-R, and *Cg*Syk-RT-F and -RT-R (Table S1), respectively. *Cg*EF (NP_001292242.2) amplified with primers *Cg*EF-RT-F and -R (Table S1) was employed as reference. The mRNA expression profiles of *Cg*IgR and *Cg*Syk in hemocytes of oysters after *V. splendidus* or LPS stimulation were detected by qRT-PCR. qRT-PCR was programmed at 95°C for 10 min, followed by 40 cycles at 95°C for 10 s, and 60°C for 45 s. The final product was analyzed via melting analysis from 65°C to 95°C. Chromatin immunoprecipitation (ChIP) was performed using antibodies against H3K4me2, and the ChIPed DNA was processed further for qRT-PCR analysis with the primer pairs (*Cg*ICP-2-PF and -PR; *Cg*LRRIG-1-PF and -PR) (Table S1). The relative expression levels were evaluated by using the $2^{-\Delta\Delta Ct}$ method (Livak and Schmittgen, 2001), and the data were statistically analyzed with *t*-text. Significant differences were accepted at $p < 0.05$.

Recombinant protein expression, purification, and antiserum production

The sequences of five Ig domains in *Cg*IgR and the TyrKc domain in *Cg*Syk were separately amplified from oyster hemocytes using the primers (*Cg*IgR-ExF and -ExR; *Cg*Syk-ExF and -ExR) (Table S1) (Sun et al., 2019). The PCR procedure was as follows: one cycle at 95°C for 3 min; 35 cycles at 94°C for 30 s, 54°C for 45 s, and 72°C for 70 s; and one cycle at 72°C for 10 min. The PCR products were inserted into the pET-30a or pET-32a expression vectors. The recombinant proteins were purified by affinity chromatography using Ni-NTA His-Bind resin following the manufacturer's instructions.

Purified recombinant proteins (100 μg) were diluted with TBS to a final volume of 100 μL then mixed with complete Freund's adjuvant (100 μL). The emulsified mixture was then subcutaneously injected into mouse four times (one injection/week). Blood samples from treated mouse were collected after the forth booster and then placed at room temperature for 4 hours to obtain the antiserum. The hemocyte samples from oyster were then used to detect the specificity of *Cg*IgR and *Cg*Syk antibody by using western blotting.

Western blotting analysis

The amino acid sequences of oyster *Cg*ERK (XP_011436159.1) and *Cg*Tubulin (NM_001305363.1) were relatively higher conserved with that of mammalian β-Tubulin. The phospho-ERK sites (GFLTEYVAT) in *Cg*ERK were identical to that of human phospho-ERK sites. The antibodies of human phospho-ERK from Cell Signaling Technology (USA) and Tubulin from Beyotime Biotechnology (China) were used for western blot assay. The

hemocyte proteins were extracted and separated by 15% SDS-polyacrylamide gel electrophoresis, and then transferred onto nitrocellulose membrane by mini transfer tank for electrophoresis. After blocked with 3% nonfat milk in TBST (10 mM Tris-HCl pH 7.5, 150 mM NaCl, 0.2% Tween-20) for 1 h, the membranes were separately incubated with 1/1000 diluted antiserum against *Cg*IgR, *Cg*Syk, *Cg*ERK, *Cg*pERK and *Cg*Tubulin in TBST with 3% nonfat milk at room temperature for 3 h. Alkaline phosphatase-conjugated goat anti-mouse IgG (Beyotime Biotechnology) (1/10,000 diluted in TBST) was incubated with the membranes at room temperature for 3 h. After washing three times, the membranes were finally dipped in the reaction system (10 mL of ddH_2O with 45 μL of NBT and 35 μL of BCIP) in the dark for about 30 min. The signal bands were imaged by Amersham Imager 600 (GE Healthcare).

Immunocytochemical assay

Four milliliters of hemolymph obtained from oysters were fixed with 4 ml of a mixture containing 2 ml of anticoagulant (pH 7.4) and 2 ml of 4% paraformaldehyde (Sun et al., 2017). The hemocytes were collected by centrifugation at 600 *g*, 4°C for 10 min, and deposited onto polylysine coated glass slide at room temperature for 40 min to adhere. The slides were washed with PBS (140 mM NaCl, 10 mM sodium phosphate, pH 7.4) and incubated in 0.2% Triton X-100 at 37°C for 5 min. After washed with PBS, the hemocytes on the glass slides were blocked with 3% BSA (30 min, 37°C) and separately incubated with anti-*Cg*IgR (1:400 in 3% BSA) at 4°C overnight. The hemocytes were then washed with PBS six times and incubated with the Alexa Fluor 488-conjugated second antibody to rabbit (Beyotime

Biotechnology; 1:1,000 ratio, diluted in 3% BSA) at 37°C in the dark for 1 h. After washed with PBS again, they were incubated with 4'-6-diamidino-2-phenylindole dihydrochloride (Beyotime Biotechnology; 1 μg mL^{-1} in PBS) at room temperature for 10 min. The slides were examined under inversion fluorescence microscope (Axio Imager A2; ZEISS).

RNA interference

The 3'-terminal sequences (about 500 bp) amplified by the primers Fi and Ri linked to the T7 promoter (Table S1) were used as templates for the dsRNA synthesis of *Cg*IgR, *Cg*Syk, *Cg*ERK, *Cg*ICP-2, and *Cg*LRRIG-1 (Sun et al., 2019). The cDNA fragment of EGFP used for dsRNA synthesis was amplified using the primers EGFP-Fi and EGFP-Ri (Table S1). The dsRNA was synthesized using T7 polymerase (Takara) at 16°C overnight according to the instruction. The *in vitro* transcription system was consisted of 2 μL 10 × transcription Buffer, 2 μL (ATP + GTP + CTP + UTP solution separately), 0.5 μL RNase inhibitor, 2 μL T7 RNA polymerase, 2 μL (1 μg) linear template DNA, and 5.5 μL RNase free dH_2O. A total of 150 oysters were employed and equally divided into six groups. The dsRNAs (50 μg) for *Cg*IgR, *Cg*Syk, *Cg*ERK, *Cg*ICP-2, *Cg*LRRIG-1 and EGFP were injected into each oyster, respectively. To enhance the RNAi effect, a second injection was performed at 12 h after the first injection. Nine oysters were sampled from each group at 24 h after the second injection and the hemolymphs collected from three individuals were pooled together as one sample. Hemocytes were collected by centrifugation at 1500 rpm, 4°C for 8 min. The total RNA of hemocytes was extracted and assessed by qRT-PCR with specific primers RT-F and RT-R

(Table S1) to evaluate the RNAi efficacy. The qRT-PCR reactions were carried out on Quan Studio 6 Flex (Thermo Fisher, USA) using SYBR premix ExTaq (RR420, Takara, Dalian). In *Cg*IgR-, *Cg*Syk- and *Cg*ERK-RNAi oysters, the mRNA transcripts of *Cg*CAICP-1 (XM_011420933.2), *Cg*ICP-2 (XM_011441342.2) and *Cg*LRRIG-1 (XM_020071501.1) in hemocytes were detected by qRT-PCR with specific primers RT-F and -R (Table S1) at 24 h after *V. splendidus* and LPS stimulations, respectively. The relative expression levels of genes were calculated as described above. The data were statistically analyzed and significant differences in the unpaired sample *t*-test were accepted at $p < 0.05$.

Recombinant protein binding assay

Gram-negative bacteria (*E. coli* and *V. splendidus*) and Gram-positive bacteria *(Staphylococcus aureus* and *Micrococcus luteus*) were used to test the binding activity of recombinant five Ig domains of *Cg*IgR with Trx-his tag (rTrx-his-5×Ig). Trx-His tag was used as control. Bacteria were cultured in 3 ml of Luria-Bertani (LB) medium (1% tryptone, 0.5% yeast extract, and 1% NaCl) overnight and collected by centrifugation at 1000 *g* for 5 min. After washed three times with TBS, the collected bacteria were resuspended in TBS and adjusted to an OD_{600} of 1.0. The bacteria suspension (400 μL) was separately incubated with 4 mM purified protein of rTrx-his-5×Ig at room temperature with rotation for 1 h. The bound proteins were dissociated from the microorganisms by loading buffer and subjected to 15% SDS-PAGE. The proteins in the gel were transferred to a nitrocellulose membrane for western blotting analysis. Anti-his antibody (1:1000 dilution in TBST containing 3% nonfat milk) was used as the primary antibody, and secondary antibody was alkaline phosphatase-conjugated

horse anti-mouse IgG (1:2000 dilution in TBST containing 5% nonfat milk).

An enzyme-linked immunosorbent assay (ELISA) was used to test the direct binding activity of rTrx-his-5×Ig to LPS from *E. coli* with His-tag as control. Each well of the microplate was coated with 2 μg of LPS and incubated at 37°C overnight. The microplate was incubated at 60°C for 30 min, blocked with bovine serum albumin (BSA) (1 mg mL^{-1}, 200 μL) at 37°C for 2 h, and washed with TBS (200 μL). The purified protein of rTrx-his-5×Ig (0, 0.001, 0.01, 0.05, 0.1, 1 and 2 μM dissolved in TBS with 0.1 mg mL^{-1} BSA) was added to each well of the coated plates and incubated at room temperature for 3 h. The plate was then washed four times with TBS, and alkaline phosphatase-conjugated horse anti-mouse IgG (1:3000 dilution in binding buffer containing 0.1 mg mL^{-1} BSA) was added (100 μL per well) and incubated at 37°C for 2 h. After the plate was washed four times with TBS, the color was developed with p-nitro-phenyl phosphate (1 mg mL^{-1} in 10 mM diethanolamine and 0.5 mM $MgCl_2$) at room temperature for 30 min. The OD value was recorded at 405 nm. Each binding assay was performed three times.

Co-immunoprecipitation (Co-IP) analysis

Proteins from oyster hemocytes were extracted with lysis buffer (150 mM NaCl, 1.0% Nonident-P40, 0.1% SDS, 50 mM Tris, pH 8.0) and incubated with protein A+G for 10 min to remove non-specific binding proteins. The proteins were separately incubated with antibodies specific for *Cg*IgR or *Cg*Syk at room temperature for 3 h, and then incubated with protein A+G at room temperature for 3 h. After washed with TBS for five times, the resulting pellet (bound protein, antibody and protein A+G) was analyzed by western blotting.

The blockage of *Cg*IgR with antibody

*Cg*IgR antibody (30 μL) was injected into the oysters with the same volume of pre-serum as control. One hour later, the *Cg*IgR-blockage oysters received an injection with 100 μL of *V. splendidus* (10^6 CFU mL^{-1}) and LPS (0.5 mg mL^{-1}), respectively. The total RNA was extracted from hemocytes, and the mRNA transcripts of *Cg*ICPs were examined by qRT-PCR. The hemocyte proteins were extracted from the treated oysters and analyzed by western blotting with anti-ERK or anti-pERK antibodies as the first antibody, respectively.

The oyster immunity was trained by twice immune stimulations

The oysters were firstly stimulated by an injection with 100 μL of *V. splendidus* (10^6 CFU mL^{-1}) or LPS (0.5 mg mL^{-1}). On the 8^{th} day after the first injection, the oysters were stimulated again with the same volume and concentration of *V. splendidus* and LPS, respectively. The mRNA transcripts of *Cg*ICPs in the hemocytes were examined at 6 h after the second injection. The phagocytosis of hemocytes in *V. splendidus* or LPS immune training oysters at 6 h after the second injection were examined by incubation with FITC-labeled *V. splendidus* and analyzed by flow cytometry and fluorescence microscope.

The treatments of R406 and PD98059

R406 (Syk inhibitor, Beyotime) and PD98059 (ERK inhibitor, Beyotime) were used to inhibit the activations of *Cg*Syk and *Cg*ERK, respectively. The oysters treated with 50 μL of R406 (0.1 μg $μL^{-1}$ diluted in PBS containing 1% DMSO) and PD98059 (0.02 μg $μL^{-1}$ diluted in

PBS containing 1% DMSO), respectively, with the same volume of 1% DMSO as control. At 1 h after the inhibitor injection, the oysters were stimulated with injections of 100 μL of *V. splendidus* and LPS, respectively. PBS was used as control. The total RNA and protein were extracted from oyster hemocytes for qRT-PCR and western blotting assays to examine the mRNA transcripts of *Cg*ICPs and phospho-*Cg*ERK, respectively.

Flow cytometry assay of the hemocyte phagocytic rates

V. splendidus (10^6 CFU mL^{-1}) were labeled with FITC (Sigma) at 37°C for 1.5 h. After twice washing with PBS and fixation in 4% paraformaldehyde for 30 min, the FITC-labeled *V. splendidus* were incubated with oyster hemocytes for 1 h, and collected by centrifugation at 600 *g*, 4°C for 5 min. The phagocytic rates of hemocytes were determined by using flow cytometry (Amnis ImageStream MKII).

Co-localization of fluorescent-labeled *V. splendidus* and lysosomes

LysoTracker Red (Beyotime) was used to stain lysosomes in oyster hemocytes following the manufacturer's protocol. The oyster hemocytes collected from three oysters were incubated with LysoTracker Red (1:20000 diluted in TBS) and FITC-labeled *V. splendidus* at room temperature for 1 h, followed by six times of washing with TBS. The hemocytes were collected and spread onto slides for observation under fluorescence microscope.

Crosslinking assay

Subric acid bis sodium salt (3-sulfo-N-hydroxysuccinimide ester, BS3; Sigma-Aldrich, USA)

is chemical compounds used for cell-surface protein crosslinking (Niu et al., 2019; Yang et al., 2016). A crosslinking assay was performed in *vivo* to detect oligomerization, according to the manufacturer's protocol. Hemocytes from oysters were collected and washed three times with ice-cold TBS. BS3 was then added to the resuspended hemocytes to a final concentration of 5 mM and the reaction mixture was incubated at 4°C for 1 h. The mixture was then terminated by adding SDS-PAGE sample loading buffer and then was treated in a boiling water bath for 8 min followed by SDS-PAGE and western blotting.

Supplemental References

Livak, K.J., and Schmittgen, T.D. (2001). Analysis of relative gene expression data using real-time quantitative PCR and the 2(-Delta Delta C(T)) Method. Methods *25*, 402-408.

Niu, G.J., Wang, S., Xu, J.D., Yang, M.C., Sun, J.J., He, Z.H., Zhao, X.F., and Wang, J.X. (2019). The polymeric immunoglobulin receptor-like protein from *Marsupenaeus japonicus* is a receptor for white spot syndrome virus infection. PLoS Pathog *15*, e1007558.

Sun, J., Wang, L., Huang, M., Li, Y., Wang, W., and Song, L. (2019). CgCLec-HTM-Mediated Signaling Pathway Regulates Lipopolysaccharide-Induced CgIL-17 and CgTNF Production in Oyster. J Immunol *203*, 1845-1856.

Sun, J.J., Lan, J.F., Zhao, X.F., Vasta, G.R., and Wang, J.X. (2017). Binding of a C-type lectin's coiled-coil domain to the Domeless receptor directly activates the JAK/STAT pathway in the shrimp immune response to bacterial infection. PLoS Pathog *13*, e1006626.

Yang, M.C., Shi, X.Z., Yang, H.T., Sun, J.J., Xu, L., Wang, X.W., Zhao, X.F., and Wang, J.X. (2016). Scavenger Receptor C Mediates Phagocytosis of White Spot Syndrome Virus and

301 Restricts Virus Proliferation in Shrimp. PLoS Pathog *12*, e1006127.